Strojniški vestnik - Journal of Mechanical Engineering vol(yyyy)no, p-p
DOI code
Original / Review / Short Scientific Paper
Received for review: yyyy-mm-dd
Received revised form: yyyy-mm-dd
Accepted for publication: yyyy-mm-dd

Synchronization and Stability of three co-rotating rotors system coupled with springs in a non-resonance system

Mingjun Du[1,*], Yongjun Hou[1], Tong Tang[2], Lian Tang[3], Faming Lei[1], Jialong Wang[1], Hongbo Gao[1],
[1] School of Mechatronics Engineering, Southwest Petroleum University, Chengdu 610500, China
[2] AECC Chengdu Engine Co. Ltd, Chengdu 610500, China
[3] Sichuan Aviation Industry Chuanxi Machinery Co., Ltd, Yaan 625100, China

With the rapid development of the horizontal drilling technology, the drilling fluid shale shaker (DFSS) will feature high capacity and high efficiency. Hence a vibrating mechanism of three co-rotating rotors system coupled with springs is proposed for designing large-sized and heavy-duty vibrating screen in petroleum drilling engineering. To master synchronization characteristic of the vibrating system, the dynamic equations of three co-rotating rotors coupled with springs are firstly built up based on Lagrange's equations. Secondly, synchronous conditions of the system are derived based on the average method, and its stability criterion is obtained by adopting Hamilton's principle. Besides, the influences of various factors including positional parameters of three motors, stiffness coefficient of the springs and frequency ratio on synchronization behavior are numerically analysed in the steady state. Additionally, the Runge–Kutta algorithm with adaptive control is employed to build an electromagnetic coupling model, and the relationships between synchronization state of the system and and its mechanical-electrical coupling characteristics are investigated. Finally, an experimental prototype is designed to prove the correctness of mentioned theory and numerical analysis. The research result shows that in-phase synchronization of three co-rotating rotors coupled with springs is easy to implement by the selection of a large enough stiffnes.

Keywords: Synchronization, Dynamic characteristic, Synchronous conditions, Stability criterion, Springs

Highlights*:*

- A vibrating mechanism of three co-rotating rotors system coupled with springs is proposed.
- The synchronization characteristics of the system are investigated by theory and numerical analysis.
- The stable phase difference of three motors are stabilized at zero by selection of a large enough stiffness.
- An experimental prototype is designed to prove the correctness of theory and numerical analysis.
- The presented model can be applied to high capacity and high efficiency in the DFSS.

0 INTRODUCTION

Vibration utilization has always played an important role in a variety of manufacturing industries, such as the vibration conveyer, vibration-impact pile driver, vibratory centrifuge, vibratory crusher, vibratory feeder, etc. The vibrating screen is the most representative vibration utilization equipment, especially in the area of petroleum drilling engineering. The vibrating scree is a kind of solids control equipment to separate out drilling cuttings from circulating drilling fluid in the process of drilling, which not only undertakes the task of removing a large number of cuttings, but also can create a necessary condition for normal operation of the next solid control equipment. A number of researches with the DFSS are focused on the study of structural design, screening performance, synchronization theory, etc. In structural design and screening performance of the vibrating screen, Baragetti put forward to increase the structural and functional performance of the screen by means of a modification of the two side-walls of the mechanical system, and studied the dynamic and structural behavior of the original and modified vibrating screen by using theoretical and numerical models [1]. Dong adopted a three-dimensional discrete element method to study the effect of aperture shape on particle flow and separation in a vibrating screen process [2, 3]. For synchronization theory of rotors, Blekhman firstly proposed the method of direct separation of motions to solve many engineering problems [4-6]. Balthazar investigated synchronization of two rotating

*Mingjun Du's Address: Southwest Petroleum University, Chengdu, China, dmj9213@163.com

unbalanced motors mounted on the horizontal beam by means of numerical simulations [7, 8]. Subsequently, Wen investigated the synchronization problem of two motors in non-resonance system via using small parameter averaging method, and various synchronous vibrating machines were invented to improve productivity [9, 10]. Based on Wen's method, Zhang et al investigated the synchronization of two or three exciters in a far-resonant vibrating system of plane motion [11, 12]. Fang et al discussed the dynamic characteristics of a rotor-pendula system by theoretical analysis and numerical simulations, and he found that the synchronous behavior is determined by mass ratio coefficients, structure parameters, rotating directions, and frequency ratios [13, 14]. Cheng et al used the average method of small parameters to explore synchronization of two eccentric rotors with a common rotational axis in the far-resonant spatial system. It can be found that the phase difference of two eccentric rotors with common rotational axis is easily approaching π during the running process of the steady-state [15, 16]. Besides, Kong and Huang studied composite synchronization of the vibrating system driven by multi-motor through applying cross-coupling control strategy and modified master-slave control structure [17-20].

Nowadays, on the one hand, with the rapid development of the horizontal drilling technology, the DFSS takes a higher demand for its processing capacity and separating efficiency. On the other hand, as the space of on-site drilling is limited, many companies have proposed to improve the processing capacity by increasing the screen layers, which caused the total mass of the vibrating body increased, and the vibrating system driven by multiple motors are required to achieve a greater exciting force. Hence, many scholars developed a vibrating system with multiple non-identical exciters in a far-resonant vibrating system to apply in DFSS [21-23]. However, for synchronization of three non-identical coupled exciters, those results prove that the phase difference of co-rotating motors stabilized in the neighborhood of Pi, and the exciting force of two exciters are counteracted each other[11]. In order to improve the amplitude and screening efficiency of the system, a vibrating mechanism of three co-rotating rotors system coupled with springs in a non-resonance system are proposed to apply for designing large-sized and heavy-duty vibrating screen in petroleum drilling engineering. In this paper, to further explore the synchronous mechanism of the proposed system and master its synchronous characteristics, the main contents are as follows: In section 1, a mechanical model of three co-rotating rotors coupled with springs is introduced. Then, the synchronous conditions and the stability criterion of the system are obtained. Next, the influence of positional parameters of three motors, stiffness coefficient of the coupling springs, frequency ratio, the total mass of the system etc., on the steady phase difference are numerical discussed in section 2. In section 3, we studied the relationships between synchronization state of the system and its mchanical-electrical coupling characteristics by utilizing the Runge–Kutta algorithm with adaptive control. In addition, an experimental prototype of three co-rotating rotors system coupled with springs is designed and manufactured. Synchronous tests and dynamic tests of the vibrating system are implemented in section 4. Finally, several important conclusions are summarized in section 5.

1 SYNCHRONIZATION MECHANISM

1.1 Mechanical model and dynamical equations

Fig. 1 shows a vibrating system driven by three co-rotating rotors coupled with springs, which mainly consists of three motors, a rigid frame, an elastic foundation, two coupling springs and four supporting springs. Unbalanced rotors actuated by three identical asynchronous motor are modeled by an eccentric lump m_i and attached eccentric length r_i $(i=1,2,3)$. Three motors are parallelly installed on a rigid frame, and the adjacent two motors are connected with a spring with a stiffness coefficient k. The distance from the rotating center of each motor to the connection of the end of coupling spring is a. And the vibrating body is connected with a fix foundation by four supporting springs with stiffness k_j and damping f_j in $j-$ direction. When three motors are simultaneously provided an electromagnetic force, the impact energy produced by its asynchronous motion is absorbed by the coupling springs during the startup stage of the system. And then the impact energy adsorbed

Strojniški vestnik - Journal of Mechanical Engineering vol(yyyy)no, p-p

DOI code
Original / Review / Short Scientific Paper
Received for review: yyyy-mm-dd
Received revised form: yyyy-mm-dd
Accepted for publication: yyyy-mm-dd

by the coupling springs is increasingly released as the operation of the vibrating system. The steady-state motion of the system is finally implemented under the action of the coupling springs. In the vibrating system, choosing $q=\left[x,y,\psi,\varphi_1,\varphi_2,\varphi_3\right]$ as a generalized coordinate. Then, the generalized active forces of the system are $Q_j=\left[0,0,0,T_{e1},T_{e2},T_{e3}\right]$ in the $-q_j$ direction. Due to the mass of three motors is far less than the rigid frame $(m_i \ll m_0)$ and the swaying displacement is extremely small $(\psi \ll 1)$, the coupling inertial moment caused by an asymmetric installation of three motors can be ignored. Considering three motors are symmetrically arranged on the rigid frame, and it's structure parameters satisfy: $l_1=l_3=l$, $l_2=l\sin\beta$, $\beta_1=\pi-\beta$, $\beta_2=\pi/2$, $\beta_3=\beta$. According to the general form of Lagrange's equation, the dynamics equations of the vibrating system are derived:

$$
\begin{aligned}
&M\ddot{x}+f_x\dot{x}+k_x x=\sum_{i=1}^{3}m_i r_i\left[\ddot{\varphi}_i\cos\varphi_i-\dot{\varphi}_i^2\sin\varphi_i\right]\\
&M\ddot{y}+f_y\dot{y}+k_y y=\sum_{i=1}^{3}m_i r_i\left[-\ddot{\varphi}_i\sin\varphi_i-\dot{\varphi}_i^2\cos\varphi_i\right]\\
&J\ddot{\psi}+f_\psi\dot{\psi}+k_\psi\psi=\sum_{i=1}^{3}m_i l_i r_i\left[\ddot{\varphi}_i\sin\left(\varphi_i+\beta_i\right)+\dot{\varphi}_i^2\cos\left(\varphi_i+\beta_i\right)\right]\\
&J_1\ddot{\varphi}_1+f_1\dot{\varphi}_1=T_{e1}+m_1r_1\ddot{x}\cos\varphi_1-m_1r_1\ddot{y}\sin\varphi_1+m_1r_1l_1\ddot{\psi}\sin\left(\varphi_1+\beta_1\right)-m_1r_1l_1\dot{\psi}^2\cos\left(\varphi_1+\beta_1\right)\\
&+ka^2\sin\left(\varphi_2-\varphi_1\right)-kla\cos\left(\varphi_1-\beta\right)+kal\sin\beta\sin\varphi_1+kl\cos\beta\, f_1\left(k,\varphi_1,\varphi_2,\beta,l,a\right)\\
&J_2\ddot{\varphi}_2+f_2\dot{\varphi}_2=T_{e2}+m_2r_2\ddot{x}\cos\varphi_2-m_2r_2\ddot{y}\sin\varphi_2+m_2r_2l_2\ddot{\psi}\sin\left(\varphi_2+\beta_2\right)-m_2r_2l_2\dot{\psi}^2\cos\left(\varphi_2+\beta_2\right)\\
&-ka^2\sin\left(\varphi_2-\varphi_1\right)+ka^2\sin\left(\varphi_3-\varphi_2\right)+kl\cos\beta\, f_2\left(k,\varphi_1,\varphi_2,\beta,l,a\right)\\
&J_3\ddot{\varphi}_3+f_3\dot{\varphi}_3=T_{e3}+m_3r_3\ddot{x}\cos\varphi_3-m_3r_3\ddot{y}\sin\varphi_3+m_3r_3l_3\ddot{\psi}\sin\left(\varphi_3+\beta_3\right)+kal\sin\beta\sin\varphi_3\\
&-m_3r_3l_3\dot{\psi}^2\cos\left(\varphi_3+\beta_3\right)-ka^2\sin\left(\varphi_3-\varphi_2\right)+kla\cos\left(\varphi_3+\beta\right)+kl\cos\beta\, f_3\left(k,\varphi_1,\varphi_2,\beta,l,a\right)
\end{aligned}
\tag{1}
$$

where

$$M=m_0+\sum_{1}^{3}m_i,\ J=J_0+\sum_{1}^{3}m_il_i^2+\sum_{1}^{3}m_ir_i^2,\ J_1=J_{o1}+m_1r_1^2,\ J_2=J_{o2}+m_2r_2^2,\ J_3=J_{o3}+m_3r_3^2$$

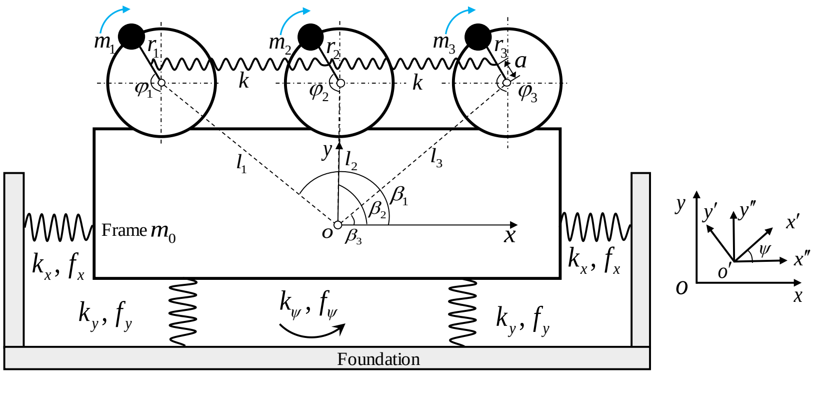

a) b)

Fig. 1. *A vibrating system driven by three co-rotating rotors coupled with springs: a) Simplified mechanical model; and b) Coordinate system*

Here, M is the total mass of the system; J is the rotational inertia of the system; $f_i\left(k,\varphi_1,\varphi_2,\beta,l,a\right)$ is a coupling term of the springs, and its expression are given in Appendix.

1.2 Steady-state response

Due to the motion of the system is changing periodically during the running process of the steady-state, the average velocity of three motors is also periodic, and their average values

*Mingjun Du's Address: Southwest Petroleum University, Chengdu, China, dmj9213@163.com

with the least common multiple period (T) are approximately equal to a constant (ω_m):

$$\omega_{\mathrm{m}} = \frac{1}{T}\int_{t_0}^{t_0+T} \dot{\varphi} dt = \text{constant} \tag{2}$$

Assuming the average phase φ of the three motors in steady state, and their phase differences are expressed by α_{12} and α_{23}, respectively, i.e. $\varphi_1 - \varphi_2 = \alpha_{12}$, $\varphi_2 - \varphi_3 = \alpha_{23}$. Hence, we have

$$\begin{aligned} &\varphi_1 = \varphi + \frac{1}{2}\alpha_{12},\ \varphi_2 = \varphi - \frac{1}{2}\alpha_{12} \\ &\varphi_3 = \varphi - \frac{1}{2}\alpha_{12} - \alpha_{23} \end{aligned} \tag{3}$$

Considering the coefficients of the instantaneous change with the average speed of three motors and their phase difference are expressed as ς_0, ς_{12}, ς_{23}, respectively. i.e.,

$$\begin{aligned} &\dot{\varphi} = \omega_m\left(1+\varsigma_0\right),\ \Delta\dot{\alpha}_{12} = \omega_m\varsigma_{12} \\ &\Delta\dot{\alpha}_{23} = \omega_m\varsigma_{23} \end{aligned} \tag{4}$$

Introducing small parameters $\varepsilon_i\ (i=1,2,3)$ to Eq. (3), we know that the vibrating system operates at the steady state when the average values $\varepsilon_i\ (i=1,2,3)$ with one period are equal to zero. Hence, the acceleration of three motors can be written as follows:

$$\begin{aligned} &\dot{\varphi}_1 = \omega_m\left(1+\varsigma_0+\frac{1}{2}\varsigma_{12}\right) = \left(1+\varepsilon_1\right)\omega_m \\ &\dot{\varphi}_2 = \omega_m\left(1+\varsigma_0-\frac{1}{2}\varsigma_{12}\right) = \left(1+\varepsilon_2\right)\omega_m \\ &\dot{\varphi}_3 = \omega_m\left(1+\varsigma_0-\frac{1}{2}\varsigma_{12}-\varsigma_{23}\right) = \left(1+\varepsilon_3\right)\omega_m \end{aligned} \tag{5}$$

And introducing following dimensionless parameters:

$$\begin{aligned} &\varsigma_x = \frac{f_x}{2\omega_{nx}M}, \varsigma_y = \frac{f_y}{2\omega_{ny}M}, \varsigma_\psi = \frac{f_\psi}{2\omega_{n\psi}J} \\ &n_j = \frac{\omega_m}{\omega_{nj}}, \eta_1 = \frac{m_1}{m_0}, \eta_2 = \frac{m_2}{m_0}, \\ &\eta_3 = \frac{m_3}{m_0},\ j = x, y, \psi \\ &r_m = \frac{m_0}{M}, l_e = \sqrt{\frac{J}{M}}, r_{li} = \frac{l_i}{l_e}, r_{ri} = \frac{r_i}{r_0},\ i = 1,2 \end{aligned} \tag{6}$$

Where,

$\omega_{nx} = \sqrt{k_x/M}, \omega_{ny} = \sqrt{k_y/M}, \omega_{n\psi} = \sqrt{k_\psi/J}$

Here, m_0 is the standard mass of the system and r_0 is the standard radius of three rotors. Inserting the dimensionless parameters (6) into Eq. (1) yields the dimensionless formulas of the dynamic equations of the system in $j-\ (j = x, y, \psi)$ direction as

$$\begin{aligned} &\ddot{x} + 2\varsigma_x\omega_{nx}\dot{x} + {\omega_{nx}}^2 x \\ &= -{\omega_m}^2 r_m r_0 \begin{bmatrix} \eta_1 r_{r1}\sin\varphi_1 + \eta_2 r_{r2}\sin\varphi_2 \\ +\eta_3 r_{r3}\sin\varphi_3 \end{bmatrix} \\ &\ddot{y} + 2\varsigma_y\omega_{ny}\dot{y} + {\omega_{ny}}^2 y \\ &= -{\omega_m}^2 r_m r_0 \begin{bmatrix} \eta_1 r_{r1}\cos\varphi_1 + \eta_2 r_{r2}\cos\varphi_2 \\ +\eta_3 r_{r3}\cos\varphi_3 \end{bmatrix} \\ &\ddot{\psi} + 2\varsigma_\psi\omega_{n\psi}\dot{\psi} + {\omega_{n\psi}}^2\psi \\ &= \frac{{\omega_m}^2 r_m r_0}{l_e}\begin{bmatrix} \eta_1 r_{l1} r_{r1}\cos\left(\varphi_1+\beta_1\right) \\ +\eta_2 r_{l2} r_{r2}\cos\left(\varphi_2+\beta_2\right) \\ +\eta_3 r_{l3} r_{r3}\cos\left(\varphi_3+\beta_3\right) \end{bmatrix} \end{aligned} \tag{7}$$

When the vibrating system operates at the steady state, the periodic solutions of the system in $j-\ (j = x, y, \psi)$ direction can be expressed as

$$\begin{aligned} &x = -r_m r_0\mu_x[\eta_1 r_{r1}\sin\left(\varphi_1-\gamma_x\right) \\ &+\eta_2 r_{r2}\sin\left(\varphi_2-\gamma_x\right) + \eta_3 r_{r3}\sin\left(\varphi_3-\gamma_x\right)] \\ &y = -r_m r_0\mu_y[\eta_1 r_{r1}\cos\left(\varphi_1-\gamma_y\right) \\ &+\eta_2 r_{r2}\cos\left(\varphi_2-\gamma_y\right) + \eta_3 r_{r3}\cos\left(\varphi_3-\gamma_y\right)] \\ &\psi = \frac{r_m r_0\mu_\psi}{l_e}[\eta_1 r_{l1} r_{r1}\cos\left(\varphi_1+\beta_1-\gamma_\psi\right) \\ &+\eta_2 r_{l2} r_{r2}\cos\left(\varphi_2+\beta_2-\gamma_\psi\right) \\ &+\eta_3 r_{l3} r_{r3}\cos\left(\varphi_3+\beta_3-\gamma_\psi\right)] \end{aligned} \tag{8}$$

here,

$$\mu_j = \frac{{n_j}^2}{\sqrt{\left(1-{n_j}^2\right)^2 + \left(2\varsigma_j n_j\right)^2}},$$

$$\gamma_j = \begin{cases} \arctan\left(\dfrac{2\varsigma_j n_j}{1-{n_j}^2}\right) & 1-{n_\psi}^2 \geq 0 \\ \pi + \arctan\left(\dfrac{2\varsigma_j n_j}{1-{n_j}^2}\right) & \text{other} \end{cases}$$

Strojniški vestnik - Journal of Mechanical Engineering vol(yyyy)no, p-p
Received for review: yyyy-mm-dd

Received revised form: yyyy-mm-dd
DOI code
Original / Review / Short Scientific Paper
Accepted for publication: yyyy-mm-dd

1.3 Synchronous conditions

Since the far-resonant vibrating system is commonly used in engineering applications, the exciting frequency of the system is 3~10 times than its natural frequency, i.e. $n_j \geq 3$, and the vibrating system with small damping $\left(\varsigma_j \leq 0.07\right)$ [10]. Hence, $\mu_j \cong n_j^{\,2} / \left(n_j^{\,2} - 1\right)$, $\gamma_j = \pi +$ $\arctan(2\varsigma_j n_j / \left(1 - n_j^{\,2}\right))$. In light of literature [11, 12], the rated slip of motors ranges from 0.02 to 0.08 during the running process of the steady-state. When three rotors are rotated with an equal velocity $\left(\dot{\varphi}_i = \omega_m\right)$, their electromagnetic torque can be written in the form:

$$T_{ei} = T_{e0i} - \bar{k}_{e0i}\bar{\varepsilon}_i \tag{9}$$

Where T_{e0i} and $\bar{k}_{e0i}$ are given in literature [14]. Differentiating Eq. (8) to obtain $\dot{x}, \ddot{x}, \dot{y}, \ddot{y}, \dot{\psi}$ and $\ddot{\psi}$. Then, inserting them into the dynamical equations of the rotors in Eq. (1), and integrating them with one period. We obtain the matrix form of $\bar{\varepsilon}_i$ in the form:

$$\mathbf{P}\dot{\bar{\boldsymbol{\varepsilon}}} = \mathbf{Q}\bar{\boldsymbol{\varepsilon}} + \boldsymbol{\mu} \tag{10}$$

where

$$\bar{\boldsymbol{\varepsilon}} = \left[\bar{\varepsilon}_1 \;\; \bar{\varepsilon}_2 \;\; \bar{\varepsilon}_3\right]^{\mathrm{T}}, \boldsymbol{\mu} = \left[\mu_1 \quad \mu_2 \quad \mu_3\right]^{\mathrm{T}}$$

$$\mathbf{P} = \begin{bmatrix} \rho_{11} & \chi'_{12} & \chi'_{13} \\ \chi'_{21} & \rho_{12} & \chi'_{23} \\ \chi'_{31} & \chi'_{32} & \rho_{13} \end{bmatrix}, \mathbf{Q} = -\omega_m \begin{bmatrix} k_{11} & \chi_{12} & \chi_{13} \\ \chi_{21} & k_{22} & \chi_{23} \\ \chi_{31} & \chi_{32} & k_{33} \end{bmatrix}$$

Parameters ρ_{11}, $\chi_{12}{}'$, etc., are shown in the Appendix.

The symbol $\mathbf{P}$ represents the coupling matrix of three rotors; the symbol $\mathbf{Q}$ is defined as the stiffness matrix of the vibrating system; and the symbol $\boldsymbol{\mu}$ is the torque coupling matrix of three rotors. When the vibrating system operates at the steady state, the coefficients of the instantaneous change are approximate to zero, i.e., $\varsigma_0 = 0$, $\varsigma_{12} = 0$, $\varsigma_{23} = 0$. Hence, the values of $\bar{\boldsymbol{\varepsilon}}$ also tends to zero. Inserting them into Eq. (10), we obtain $\boldsymbol{\mu} = 0$, and adding them together to get following expression:

$$\begin{aligned}
&\sum_{i=1}^{3} T_{e0i} - \omega_m \sum_{i=1}^{3} f_i \\
&-\frac{1}{2} m_0 r_0^{\,2} \omega_m^{\,2} \sum_{i=1}^{3} \left(\eta_i^{\,2} r_{ri}^{\,2} W_{si}\right) + kl\cos\beta F\left(\alpha_{12}, \alpha_{23}\right) / 2\pi \\
&+\frac{1}{2} m_0 r_0^{\,2} \omega_m^{\,2} \eta_1 \eta_3 r_{r1} r_{r3} \begin{bmatrix} -W_{s13}\sin\left(\alpha_{12} + \alpha_{23} + \theta_{s13}\right) \\ -W_{s13}\cos\left(\alpha_{12} + \alpha_{23} + \theta_{s13}\right) \end{bmatrix} \\
&-m_0 r_0^{\,2} \omega_m^{\,2} \eta_2 \eta_3 r_{r2} r_{r3} W_{s23} \cos\left(\alpha_{23} + \theta_{s23}\right) \\
&-m_0 r_0^{\,2} \omega_m^{\,2} \eta_1 \eta_2 r_{r1} r_{r2} W_{s12} \cos\left(\alpha_{12} + \theta_{s12}\right) = 0
\end{aligned} \tag{11}$$

where

$$\begin{aligned}
&F\left(\alpha_{12}, \alpha_{23}\right) \\
&= \int_0^{2\pi} \frac{-2la\cos\beta\sin\dfrac{\alpha_{12}}{2}\sin\varphi}{\begin{bmatrix} l^2\cos^2\beta + 2a^2 - 2a^2\cos\alpha_{12} \\ +4la\cos\beta\sin\dfrac{\alpha_{12}}{2}\cos\varphi \end{bmatrix}^{0.5}} d\varphi \\
&+ \int_0^{2\pi} \frac{-2la\cos\beta\sin\dfrac{\alpha_{23}}{2}\sin\left(\varphi - \dfrac{\alpha_{12} + \alpha_{23}}{2}\right)}{\begin{bmatrix} l^2\cos^2\beta + 2a^2 - 2a^2\cos\alpha_{23} \\ +4la\cos\beta\sin\dfrac{\alpha_{23}}{2}\cos\left(\varphi - \dfrac{\alpha_{12} + \alpha_{23}}{2}\right) \end{bmatrix}^{0.5}} d\varphi
\end{aligned}$$

Eq. (11) is the equilibrium equation of the dynamical moment of whole system. The first term $\left(\sum_{i=1}^{3} T_{e0i}\right)$ represents the sum of the output torque of three motors; the second term $\left(\omega_m \sum_{i=1}^{3} f_i\right)$ is the sum of resistance torque of three motors during operation; and the remaining terms denote the mechanical load of three motors operating in the steady state and the coupling torque of those connecting springs among three rotors. Moreover, it can be seen that there is no coupling term with connecting spring in Eq. (11). An optimal zero phase synchronization of three motors are achieved, i.e., $\alpha_{12} = 0$, $\alpha_{23} = 0$. That is to say the deformation rate of this connecting springs is always equal to zero during the running process of the steady-state. Due to $\boldsymbol{\mu} = 0$, the difference equations of two of motors can be obtained:

*Mingjun Du's Address: Southwest Petroleum University, Chengdu, China, dmj9213@163.com

$$
\begin{aligned}
&\left[T_{e01}-\omega_m f\right]-\left[T_{e02}-\omega_m f_2\right]+ka^2\left[\sin\alpha_{23}-2\sin\alpha_{12}\right]\\
&+\frac{kl\cos\beta}{2\pi}\left[F_1(\varphi)-F_2(\varphi)\right]\\
&+\frac{1}{2}m_0 r_0^{\,2}\omega_m^{\,2}\begin{bmatrix}-\eta_1^{\,2}r_{r1}^{\,2}W_{s1}+\eta_2^{\,2}r_{r2}^{\,2}W_{s2}\\ -2\eta_1\eta_2 r_{r1}r_{r2}W_{c12}\sin\left(\alpha_{12}+\theta_{c12}\right)\end{bmatrix}\\
&-\frac{1}{2}m_0 r_0^{\,2}\omega_m^{\,2}\eta_1\eta_3 r_{r1}r_{r3}\begin{bmatrix}W_{c13}\sin\left(\alpha_{12}+\alpha_{23}+\theta_{c13}\right)\\ +W_{s13}\sin\left(\alpha_{12}+\alpha_{23}+\theta_{s13}\right)\end{bmatrix}\\
&+\frac{1}{2}m_0 r_0^{\,2}\omega_m^{\,2}\eta_2\eta_3 r_{r2}r_{r3}\begin{bmatrix}W_{c23}\sin\left(\alpha_{23}+\theta_{c23}\right)\\ +W_{s23}\cos\left(\alpha_{23}+\theta_{s23}\right)\end{bmatrix}=0
\end{aligned}
\tag{12}
$$

$$
\begin{aligned}
&\left[T_{e02}-\omega_m f_2\right]-\left[T_{e03}-\omega_m f_3\right]\\
&+ka^2\left[\sin\alpha_{12}-2\sin\alpha_{23}\right]+\frac{kl\cos\beta}{2\pi}\left[F_2(\varphi)-F_3(\varphi)\right]\\
&+\frac{1}{2}m_0 r_0^{\,2}\omega_m^{\,2}\eta_1\eta_2 r_{r1}r_{r2}\begin{bmatrix}W_{c12}\sin\left(\alpha_{12}+\theta_{c12}\right)\\ -W_{s12}\cos\left(\alpha_{12}+\theta_{s12}\right)\end{bmatrix}\\
&+\frac{1}{2}m_0 r_0^{\,2}\omega_m^{\,2}\begin{bmatrix}-\eta_2^{\,2}r_{r2}^{\,2}W_{s2}+\eta_3^{\,2}r_{r3}^{\,2}W_{s3}\\ -2\eta_2\eta_3 r_{r2}r_{r3}W_{c23}\sin\left(\alpha_{23}+\theta_{c23}\right)\end{bmatrix}\\
&-\frac{1}{2}m_0 r_0^{\,2}\omega_m^{\,2}\eta_1\eta_3 r_{r1}r_{r3}\begin{bmatrix}W_{c13}\sin\left(\alpha_{12}+\alpha_{23}+\theta_{c13}\right)\\ -W_{s13}\cos\left(\alpha_{12}+\alpha_{23}+\theta_{s13}\right)\end{bmatrix}\\
&=0
\end{aligned}
\tag{13}
$$

Eq. (12) and Eq. (13) are dimensionless difference equations with respect to α_{12} and α_{23}, which reveals coupling property of the system when the vibrating system operates at the steady state.

1.4 Stability criterion

In this study, neglecting the effect of system damping, the vibrating system is suffering not only gravitational forces but also the output torque of motors during the running process of the steady-state. Thereby, three co-rotating rotors system coupled with springs is a nonholonomic conservation system. According to the Hamilton's principle, we get following expression:

$$\int_0^{2\pi}\left[\delta\left(T-V\right)+\sum_{i=1}^{3}Q_i\delta q_i\right]\mathrm{d}\varphi=0 \tag{14}$$

Where T, V, Q_i and q_i represent the total kinetic energy, the total potential energy, the generalized force, and the generalized coordinate of the system, respectively. From the model proposed in Fig. 1, we obtain total kinetic energy of the system:

$$T=\frac{1}{2}m_0\left(\dot{x}^2+\dot{y}^2\right)+\frac{1}{2}J_0\dot{\psi}^2+T_z \tag{15}$$

Here T_z is the sum of kinetic energy with three motors. Since their rotation speed are identity with each other during the running process of the steady-state, T_z can be regarded as a constant. The total potential energy of the vibrating system can be written as:

$$
\begin{aligned}
V&=\frac{1}{2}k_x x^2+\frac{1}{2}k_y y^2\\
&+\frac{1}{2}k_\psi\psi^2+\frac{1}{2}k\Delta_1^{\,2}+\frac{1}{2}k\Delta_2^{\,2}
\end{aligned}
\tag{16}
$$

The interaction Hamiltonian of the system over one period can be written the following:

$$H=\int_0^T\left(T-V\right)dt=\int_0^{2\pi}\left(T-V\right)d\varphi \tag{17}$$

As the model of three co-rotating rotors system has two degree of freedoms (DOFs), we choose $\Delta\alpha_{12}$, $\Delta\alpha_{23}$ to be a generalized coordinate. Three rotors are rotating with an equal velocity$\left(\omega_m\right)$ when the vibrating system operates at the steady state. Simultaneously, the values of $\Delta\alpha_{12}$ and $\Delta\alpha_{23}$ are approximately equal to a constant ($\Delta\alpha_{12}^{\;*}$ and $\Delta\alpha_{23}^{\;*}$). According to a mechanic system with integrity constraint, the system can be changed from one position to anther under the action of conservative forces, and the movement of the system is tending to be stable when its interaction Hamiltonian has a minimum. Therefore, a stability criterion of the system can be obtained in the form:

$$
\begin{aligned}
&\frac{\partial^2 H}{\partial\Delta\alpha_{12}^{\;2}}>0\\
&\frac{\partial^2 H}{\partial\Delta\alpha_{12}^{\;2}}\bullet\frac{\partial^2 H}{\partial\Delta\alpha_{23}^{\;2}}-\left(\frac{\partial^2 H}{\partial\Delta\alpha_{12}\partial\Delta\alpha_{23}}\right)^2>0
\end{aligned}
\tag{18}
$$

2 NUMERICAL DISSCUSSION

Some theoretical results with regard to synchronous conditions and stability criterion for three co-rotating rotors system coupled with springs are described in the preceding section. From Eqs.(12), (13) and (18), it can be seen that synchronous state of the system is mainly

Strojniški vestnik - Journal of Mechanical Engineering vol(yyyy)no, p-p
© 2015 Journal of Mechanical Engineering. All rights reserved.
DOI code
Original / Review / Short Scientific Paper
Received for review: yyyy-mm-dd
Received revised form: yyyy-mm-dd
Accepted for publication: yyyy-mm-dd

determined by positional parameters of three motors, stiffness coefficient of the coupling springs, frequency ratio, the total mass of the system, etc. To deeply grasp the influence of various factors on synchronous state of the system, some numerical analysis for solving Eq. 12 and Eq. 13 under the conditions of Eq. (18) are performed to analyse the influence of positional parameters of three motors and frequency ratio on synchronous characteristic of the vibrating system.

When the vibrating system operates at the steady state, the synchronization state of the system is defined as follows: The phase difference of rotors is always close to $(-\pi/2, \pi/2)$ or $(-90^{\circ}, 90^{\circ})$, the vibrating system is called the in-phase synchronization. And the phase difference of rotors is always close to $(\pi/2, 3\pi/2)$ or $(90^{\circ}, 270^{\circ})$, the system is called the anti-phase synchronization. Considering installation angle β of motors are set as15°, 30°, 42°, 60°, respectively, and the influence of stiffness coefficient of the coupling springs on synchronization state are presented in Fig. 2. When $k=0$, that is to say there isn't coupling springs among these rotors, the phase differences between $2\alpha_{12}$ and $2\alpha_{23}$ consistently tend towards anti-phase synchronization. From Fig. 2(c), it can be found that the values of $2\alpha_{12}$ and $2\alpha_{23}$ are equal to 127.4° and 112.1°, respectively, when $\beta = 42^{\circ}$. For the coupling springs with a small coefficient, their elastic force has no influence on synchronous characteristic of the vibrating system. But with the increasing of k over a critical value, the phase difference between each pair of the rotors gradually stabilize at zero. Accordingly, the synchronous state of the system is changed from anti-phase synchronization to the in-phase synchronization suddenly. Moreover, from contrasting results shown in Fig. 2, it is also demonstrated installation angles of three motors have significantly impacted on synchronous behavior of the vibrating system.

Table 1. *The structural parameters of the vibrating system in engineering*

unbalanced rotors $i=1,2,3$	a rigid frame	motor	coupling springs
$m_i = 2$ (kg)	$M = 90$ (kg)	$l_1 = 0.35, 0.52,$	$k = 1 \sim 4.2\times10^4$ (N/m)
$r = 0.04$ (m)	$J = 6.8$ (kg.m2)	$0.64, 0.85$ (m)	$a = 0.02$ (m)
$\omega_m = 157$ (rad/s)	$k_x = 8\times10^4, 6.6\times10^6$ (N/m)	$l_2 = 0.12, 0.18,$	—
$f_i = 0.02$ (N.s/m)	$k_y = 8\times10^4, 6.6\times10^6$ (N/m)	$0.22, 0.3$ (m)	—
—	$k_\psi = 6\times10^3, 4.96\times10^5$ (N/m)	$l_3 = 0.35, 0.52,$	—
—	$f_x = 1000$ (N.s/m)	$0.64, 0.85$ (m)	—
—	$f_y = 1000$ (N.s/m)	$\beta_1 = 160^{\circ}$	—
—	$f_\psi = 1000$ (N.s/m)	$\beta_2 = 78^{\circ}$	—
—	—	$\beta_3 = 20^{\circ}$	—

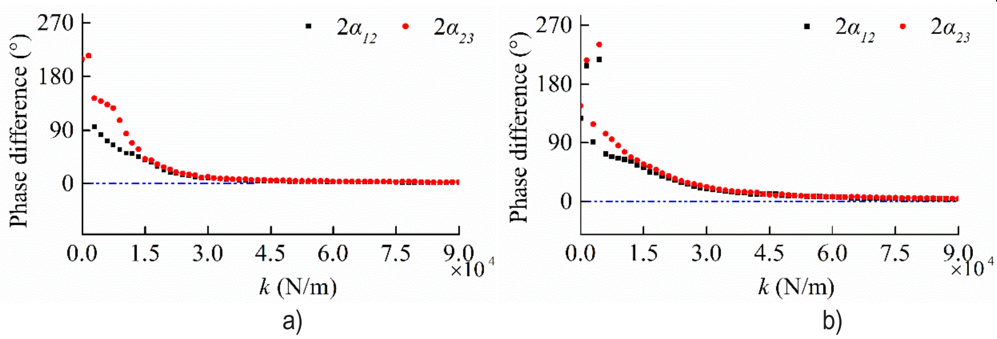

*Mingjun Du's Address: Southwest Petroleum University, Chengdu, China, dmj9213@163.com

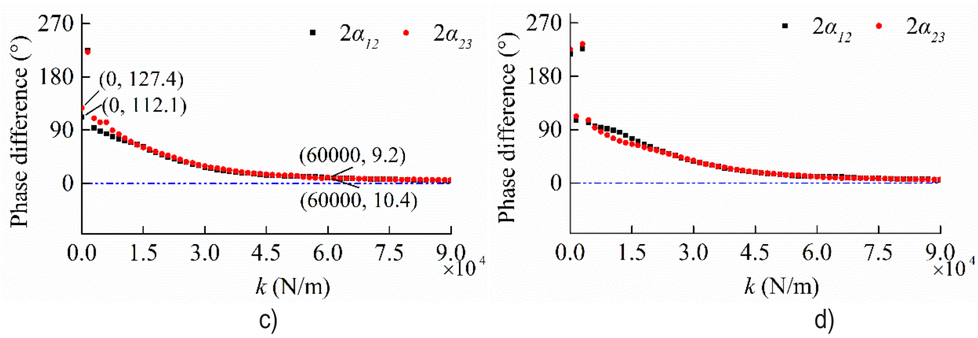

Fig. 2. *Installation angle of motors and stiffness coefficient of the coupling springs are major influence on the dynamic characteristics: a) $\beta = 15°$; b) $\beta = 30°$; c) $\beta = 42°$; and d) $\beta = 60°$*

We assume that $\beta = 42^{\circ}$ and the value of l is equal to 0.32[m], 0.64[m], 0.85[m], 1.28[m], respectively. The influences of stiffness coefficient of the coupling springs on synchronization state are illustrated in Fig. 3. Compared with numerical results with different installation distances, the parameter l has an appreciably effect on synchronous behavior of the vibrating system when $k = 0$. In addition, anti-phase synchronization occurs for the coupling springs with a small coefficient. But with the increasing k over a critical value, the phase difference between each pair of the rotors gradually stabilize at zero. Accordingly, it can be concluded that the changing trends closing to zero are different when three motors are installed in different location.

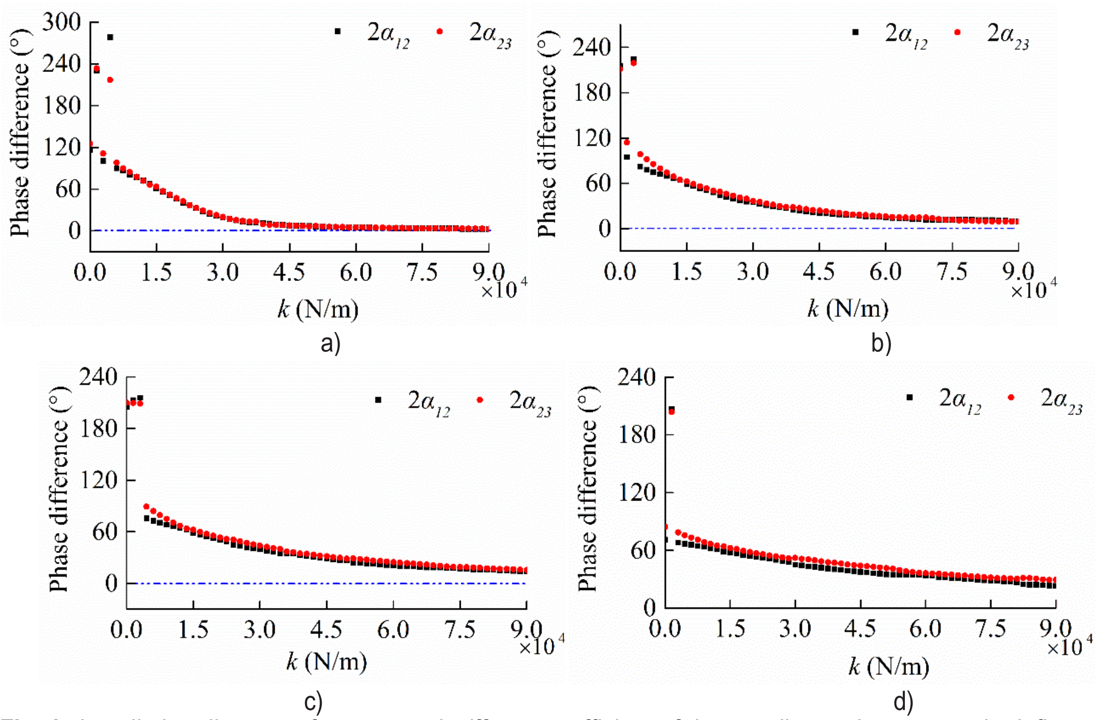

Fig. 3. *Installation distance of motors and stiffness coefficient of the coupling springs are major influence on the dynamic characteristics:a) $l = 0.32$ [m]; b) $l = 0.64$ [m]; c) $l = 0.85$ [m]; and d) $l = 1.28$ [m]*

Fig. 4 shows stiffness coefficient of the coupling springs is major influence on the dynamic characteristics of the vibrating system under the conditions of different frequency ratio. It can be concluded that frequency ratio of the system has no influence on synchronous behavior.

Strojniški vestnik - Journal of Mechanical Engineering vol(yyyy)no, p-p

DOI code
Original / Review / Short Scientific Paper
Received for review: yyyy-mm-dd
Received revised form: yyyy-mm-dd
Accepted for publication: yyyy-mm-dd

But for different frequency ratio, the changing rule of phase difference with changing of stiffness coefficient of the coupling springs in the steady state are consistent with those preceding conclusions in Fig. 2 and Fig. 3.

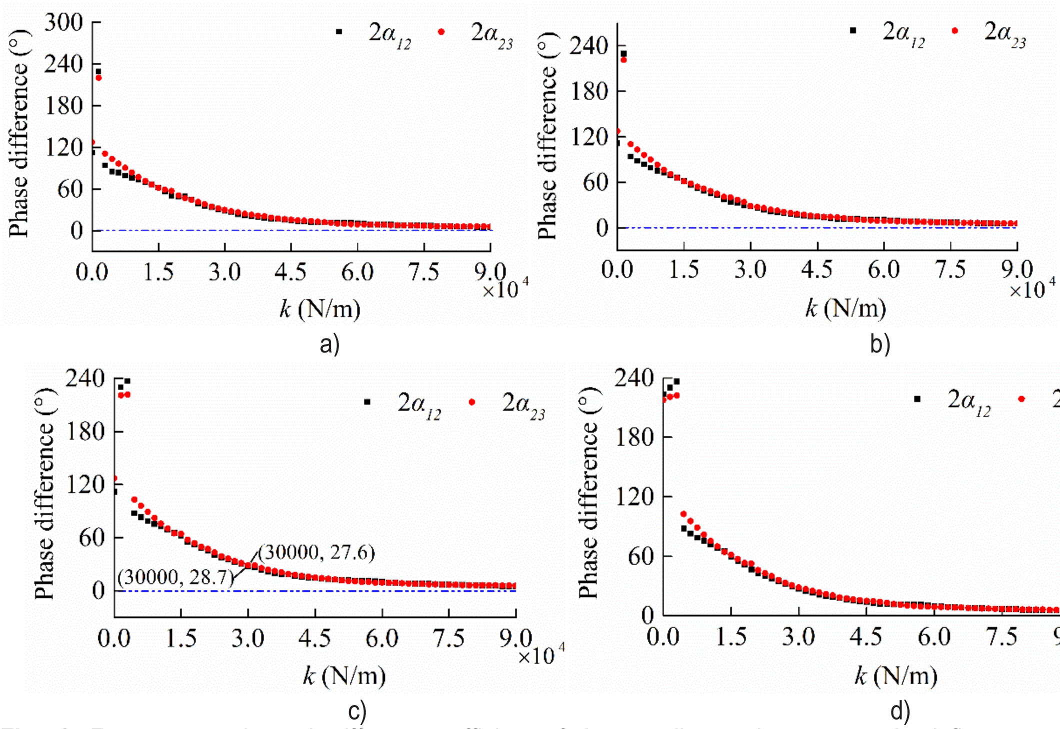

Fig. 4. *Frequency ratio and stiffness coefficient of the coupling springs are major influence on the dynamic characteristics: a)* $n_j = 4.47$ *; b)* $n_j = 5$ *; c)* $n_j = 6.8$ *; and d)* $n_j = 8.95$

3 SIMULATION VERIFICATION

Based on the dynamics equations (1), a simulation model with three co-rotating rotors system coupled with springs are established by means of the Runge–Kutta algorithm with adaptive control. The relationships between synchronization state of the system and their mechanical-electrical coupling characteristics are investigated, and further analysis results are employed to verify the correctness of theoretical derivation and numerical analysis. Simulation parameters are identical with numerical results in Table 1.

3.1 Dynamic characteristics for $K = 0$ [N/m], $l = 0.48$ [m], $n_j = 5.48$

Simulation results for $n_j(j = x, y, \psi) = 5.48$, $l = 0.48$ [m], $k = 0$ [N/m] are shown in Fig. 5. Here, $k_x = 8\times10^4\,[\mathrm{N/m}]$ $k_y = 8\times10^4\,[\mathrm{N/m}]$, $k_\psi = 1.28\times10^4$ [rad/m]. The vibrating system are gradually changed from desynchrony state to the synchronization for about 3 seconds, and the driving torque of three motors are changed near 3.9[N.m], 3.71[N.m], 3.71[N.m], respectively, as shown in Fig. 5(a). Moreover, three rotors are rotated with a same velocity 152.7[rad/s] when the vibrating system operate at the steady state, the phase difference $2\alpha_{12}$ between rotor1 and rotor 2 is stabilized at -4.49[rad] ($102.7^\circ \triangleq -4.49[\mathrm{rad}]$ $+2\pi$) and the phase difference $2\alpha_{23}$ between rotor2 and rotor 3 is stabilized at 8.42[rad](122.4° ≙ 8.42[rad] -2π), as shown in Fig. 5(f). Compared with numerical result of the corresponding parameter in Figure2(c), the results show that simulation results are proven to be in good agreement with numerical results. Fig 5(c), 5(d) and 5(e) shows phase diagrams of the vibrating system in the DOFs. As seen from those diagrams, the rigid frame was't rapidly excitated

*Mingjun Du's Address: Southwest Petroleum University, Chengdu, China, dmj9213@163.com

owing to its large mass during the initial process of the vibrating system, which caused the phase diagram of the mass center of the system are chaotic in the DOFs. The synchronous behavior of vibrating system is gradually implemented as the system kept running, the phase diagram of the mass center of the system in the x-y plane is a closed ellipse, and its amplitude in the DOFs is 2.82×10^{-3}[m], 2.8×10^{-4}[m], 3.34×10^{-4}[rad], respectively, as schematically illustrated in Fig. 5(g).

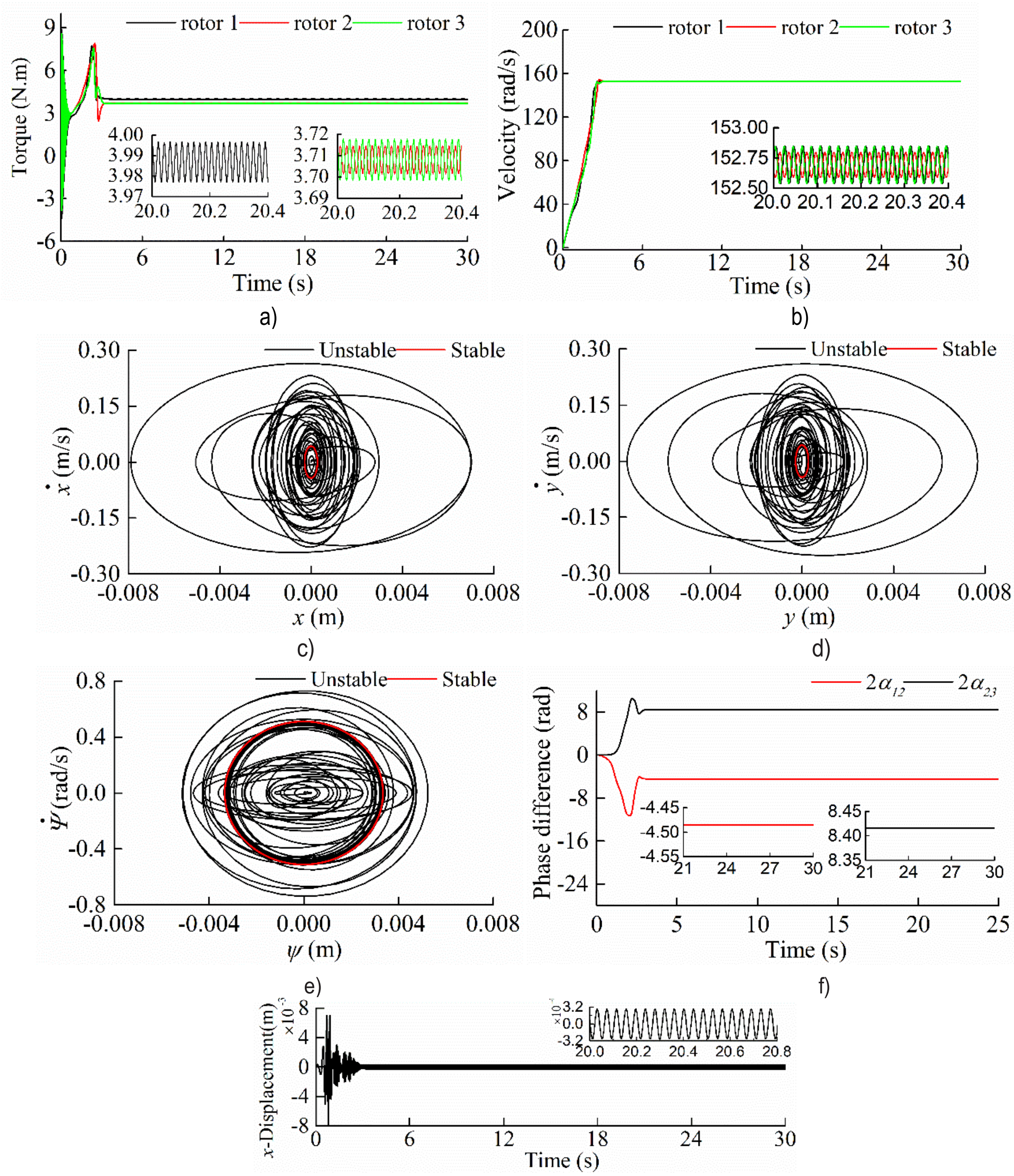

Strojniški vestnik - Journal of Mechanical Engineering vol(yyyy)no, p-p

DOI code
Original / Review / Short Scientific Paper
Received for review: yyyy-mm-dd
Received revised form: yyyy-mm-dd
Accepted for publication: yyyy-mm-dd

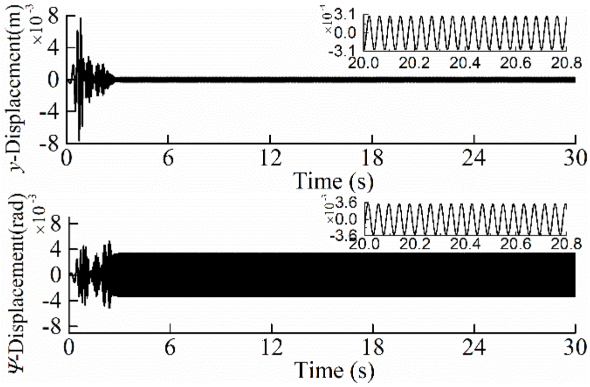

g)

Fig. 5. *Simulation results for $k = 0$ [N/m], $l = 0.48$ [m], $n_j = 5.48$; a) Driving torque of three motors; b) rotational velocity of three motors; c) Phase diagram of the system in $x-$ direction; d) Phase diagram of the system in $y-$ direction; e) Phase diagram of the system in $\psi-$ direction; f) Phase difference of three motors; and g) Displacement response of the rigid frame in $x-$, $y-$, $\psi-$ directions, respectively*

3.2. Dynamic characteristics for $K = 60000[\mathrm{N/m}]$, $l = 0.48[\mathrm{m}]$, $n_j = 5.48$

For system parameters in section 4.1, changing the value $k = 6\times10^4$ [N/m], and simulation results are shown in Fig. 6. When three motors are simultaneously provided with electromagnetic force, the synchronization phenomenon occurs after 4 seconds, and the rotational velocities of three motors are stabilize at 151.8[rad/s], as shown in Fig. 6(b). As illustrated in Fig. 6(a), the driving torque of three motors in synchronous state are 4.72[N.m], 4.4[N.m], 4.4[N.m], respectively. Fig 6(c), 6(d) and 6(c) show phase diagrams of the vibrating system in $x-$, $y-$ and $\psi-$ directions, respectively. The results show that the phase diagram of the mass center of the system are chaotic during the initial process of the vibrating system. And its phase diagra in the x-y plane is a closed ellipse when the vibrating system operates at the steady state. The value of $2\alpha_{12}$ is approximately equal to 0.194[rad] ($11.1° \triangleq 0.194[\mathrm{rad}]$) , and the value of $2\alpha_{23}$ is approximately equal to 0.181[rad] ($10.4° \triangleq 0.181[\mathrm{rad}]$) . By comparison, the simulation results are in good agreement with numerical results. Fig. 6(g) shows the amplitude of the mass center of the system in synchronous state, and its magnitudes are 3.1×10^{-3}[m], 3.1×10^{-3}[m], 4.64×10^{-3}[rad], respectively, as shown in Table 2. In addition, comparing simulation results in Fig. 5 and Fig. 6, it is demonstrated that synchronous state of the system is significantly changed by those coupling springs among the rotors, which makes the system transit from anti-phase synchronization to the in-phase synchronization. And it can be seen that adjusting the value of the coupling spring stiffness can make phase difference close to zero to meet the requirements of the strongly exciting designing large-sized and heavy-duty vibrating screens in engineering.

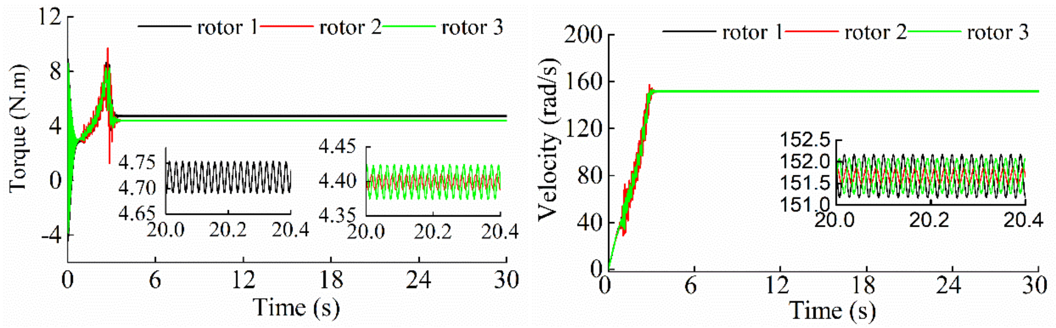

*Mingjun Du's Address: Southwest Petroleum University, Chengdu, China, dmj9213@163.com

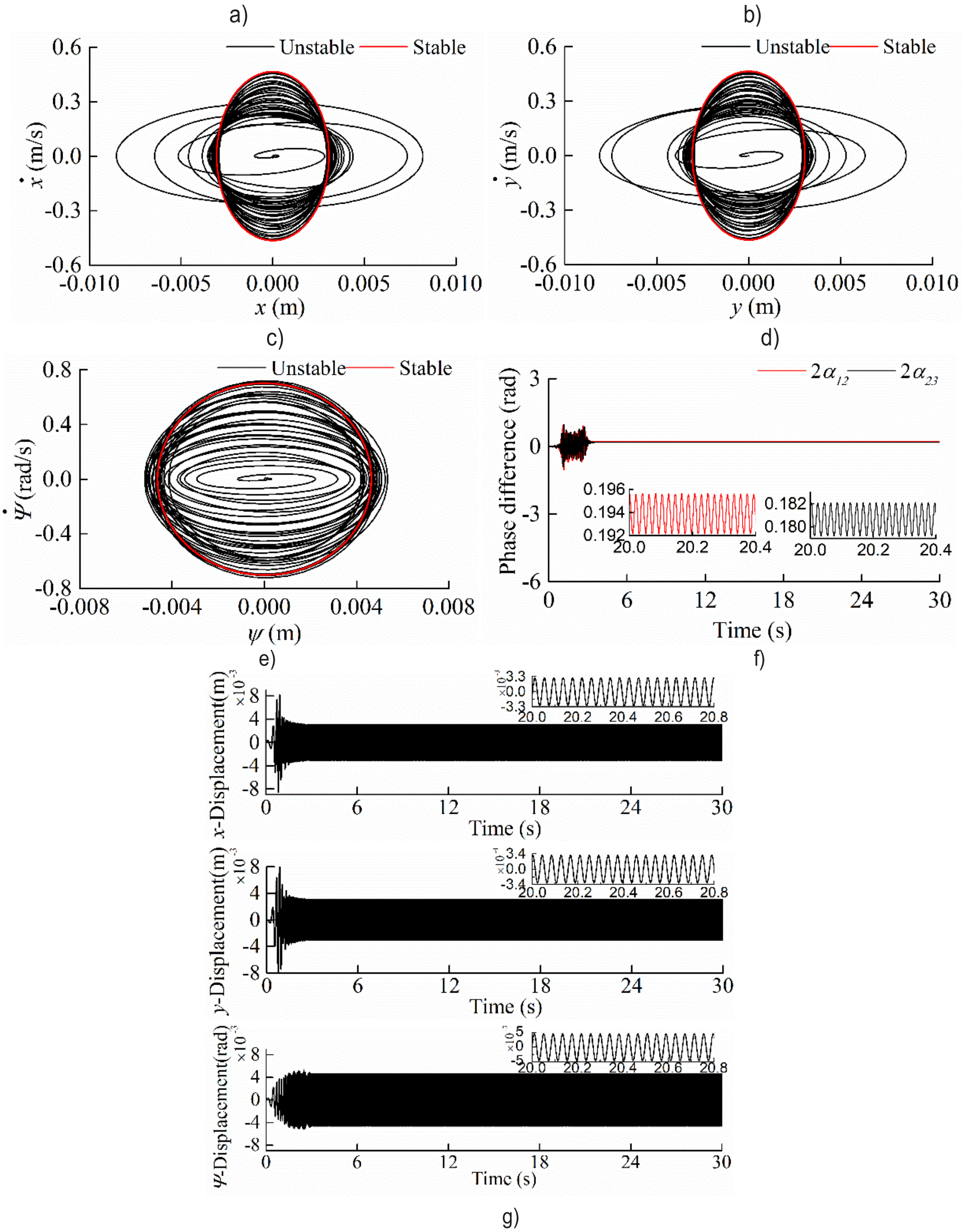

Fig. 6. *Simulation results for* $k = 60000$ *[N/m],* $l = 0.48$ *[m],* $n_j = 5.48$*: a) Driving torque of three motors; b) Rotational velocity of three motors; c) Phase diagram of the system in* $x-$ *direction; d) Phase diagram of the system in* $y-$ *direction; e) Phase diagram of the system in* $\psi-$ *direction; f) Phase difference of three motors; and g) Displacement response of the rigid frame in* $x-$ *,* $y-$ *,* $\psi-$ *directions, respectively*

Strojniški vestnik - Journal of Mechanical Engineering vol(yyyy)no, p-p

DOI code
Original / Review / Short Scientific Paper
Received for review: yyyy-mm-dd
Received revised form: yyyy-mm-dd
Accepted for publication: yyyy-mm-dd

Table 2. Displacement amplitude of the vibrating system with the changing of the stiffness of the coupling springs

	$x-$direction (mm)	$y-$direction (mm)	$\psi-$ direction (mm)
$k=0$	2.82	0.28	3.34
$k=60000$	3.1	3.1	4.64

3.3. Dynamic characteristics for $K=30000[\mathrm{N/m}]$, $l=0.48[\mathrm{m}]$, $n_j=6.8$

Fig. 7 presents results of computer simulation when $k=30000$ [N/m], $l=0.48$ [m], $n_j=6.8$. Here, $k_x=k_y=5.2\times10^4$ [N/m], $k_\psi=8.32\times10^3$[rad/m]. The synchronous velocity of three rotors is rotating with a speed 152.5[rad/s] while the vibrating system operates at the steady state, and their output torques are stabilized at 4.28[N.m], 3.99[N.m], 3.99[N.m], respectively. The value of $2\alpha_{12}$ is 0.58[rad](33.2° ≙ 0.58[rad]), and the value of $2\alpha_{23}$ is 0.523[rad] (29.97°≙ 0.523[rad]). Thus, the simulation results are in good agreement with the numerical results discussed in Fig. 7 and Fig. 5. Fig. 7(g) shows the amplitude of the mass center of the system in synchronous state, and its magnitudes are 3×10^{-3}[m], 2.9×10^{-3}[m], 3×10^{-3}[rad], respectively.

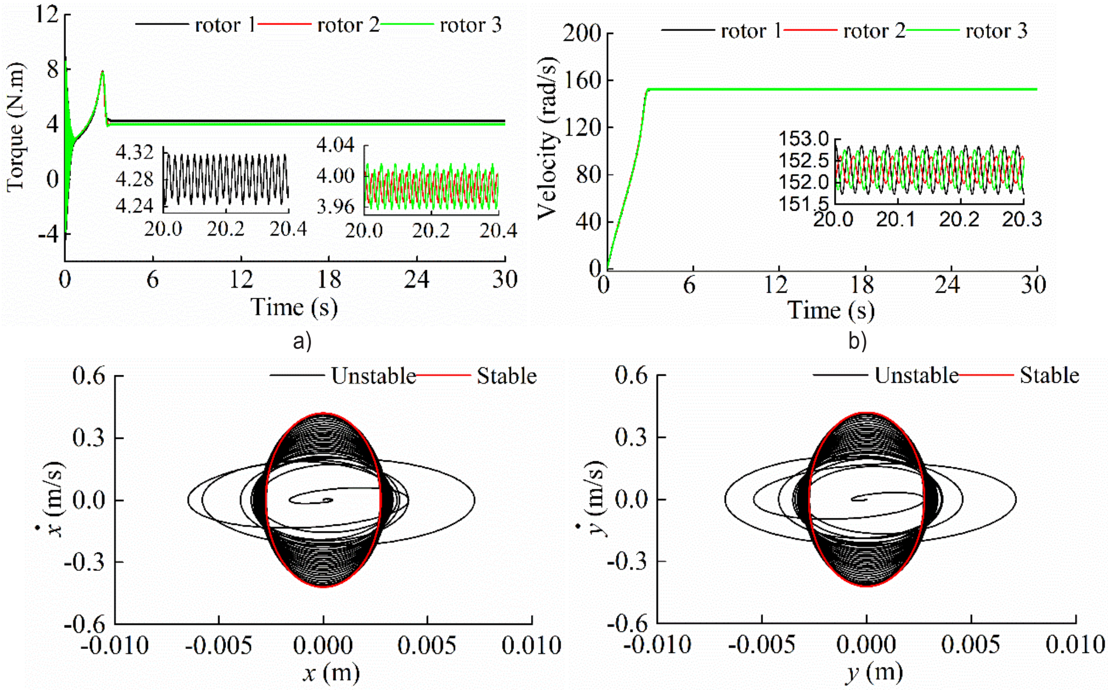

a)
b)
c)
d)

*Mingjun Du's Address: Southwest Petroleum University, Chengdu, China, dmj9213@163.com

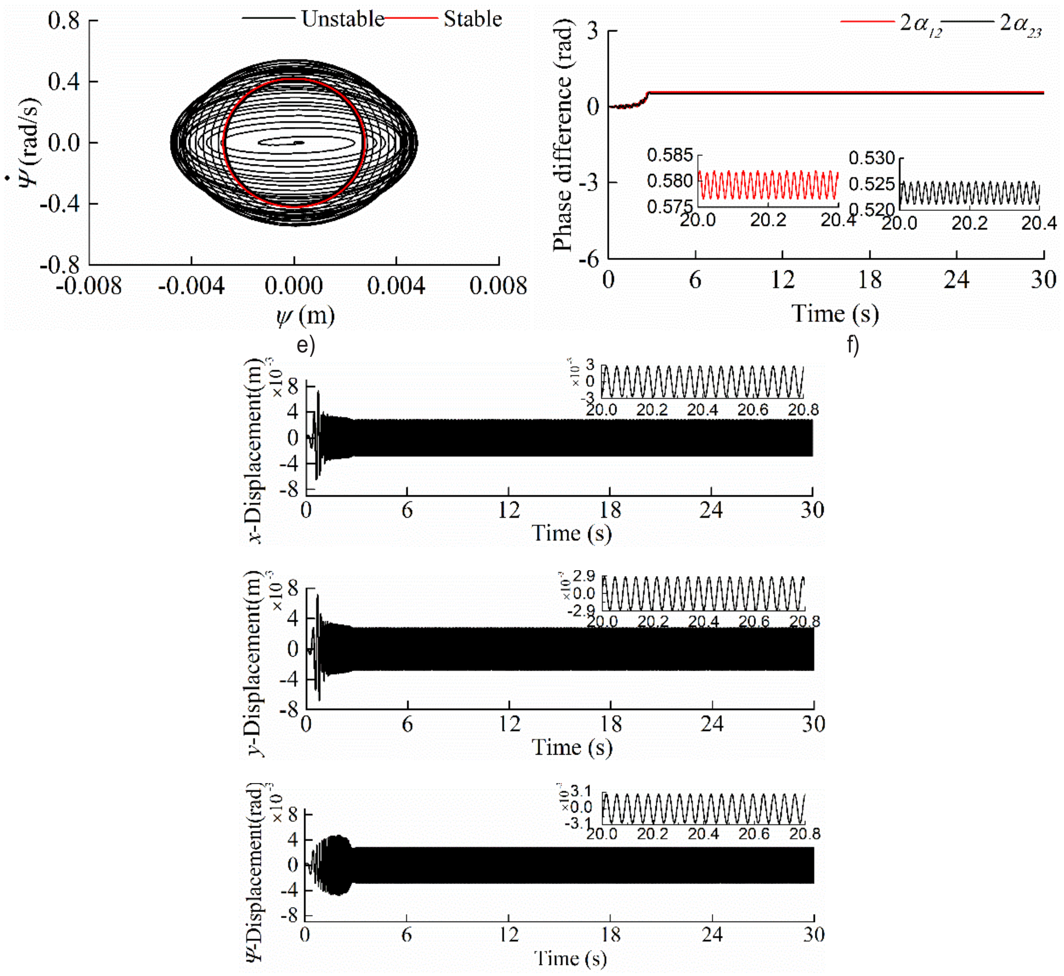

g)

Fig. 7. *Simulation results for* $k = 30000$ *[N/m],* $l = 0.48$ *[m],* $n_j = 6.8$ *: a) Driving torque of three motors; b) Rotational velocity of three motors; c) Phase diagram of the system in* $x-$ *direction; d) Phase diagram of the system in* $y-$ *direction; e) Phase diagram of the system in* $\psi-$ *direction; f) Phase difference of three motors; and g) Displacement response of the rigid frame in* $x-$*,* $y-$*,* $\psi-$ *directions, respectively*

4 EXPERIMENTAL VERIFICATION

To validate the correctness of above-mentioned theory and numerical analysis, it is necessary to further give some corresponding experimental analyses. An experimental strategy with synchronous tests and dynamic tests of the vibrating system are introduced, which consists of high-speed imaging system and dynamic testing system. The experimental prototype including induction motors(YZS-1.5-4), coupling springs, a rigid frame, an elastic foundation, four supporting springs, etc., are shown in Fig. 8. The motor performance parameters of YZS-1.5-4 are shown in Table 3. Two inseries springs in the coupling springs have always subjecting to a changing force alternately in compression when the vibrating system operates at the steady state, which ensured three rotors rotating in the same directions are easy to achieve a in-phase synchronization. The main parameters of the experimental prototypes are $l_1 = 0.41$ [m], $l_2 = 0.15$ [m], $l_3 = 0.4$ [m], $\beta_1 = 159^{\circ}$, $\beta_2 = 83^{\circ}$, and the other parameters are identical with table 1. The location parameters of four measuring

Strojniški vestnik - Journal of Mechanical Engineering vol(yyyy)no, p-p

DOI code
Original / Review / Short Scientific Paper
Received for review: yyyy-mm-dd
Received revised form: yyyy-mm-dd
Accepted for publication: yyyy-mm-dd

point on the prototype are $P_1(-0.45,-0.23)$, $P_2(-0.22,-0.23)$, $P_3(0.23,-0.23)$, $P_4(0.46,-0.23)$, respectively.

a) b)

Fig. 8. *Experimental prototypes: a) three co-rotating rotors in a vibrating system; and b) two co-rotating rotors coupled with two inseries springs*

Table 3 . Parameters for vibration three-phase asynchronousmotor (YZS-1.5-4)

Parameter	Voltage [V]	Power rating [HZ]	Output Power [kw]	Current [A]	Frequency [r/min]	Exciting force [kN]	Weight [kg]
Value	380	50	0.12	0.36	1500	1.5	16

The dynamic testing results of three co-rotating rotors in a vibrating system are shown in Fig. 9. From spectral analyse shown in Fig. 9(a), it can be seen that the peak spectra of point P_2 and point P_3 in horizontal and vertical directions reaches a maximum when system frequency is approximately equal to 24.125 [Hz]. Fig 9(b) and 9(c) show acceleration of four measuring point in horizontal and vertical directions. It can be concluded that their magnitudes are almost the same with a value 24.4[m/s^2]. But the phase constants of the acceleration with point 1 and 4 are different than point 2 and 3 in horizontal direction, and both the magnitudes and phase constants of their acceleration are different in vertical direction. Fig 9(d) and 9(e) show velocity of four measuring point in horizontal and vertical directions, and Fig 9(f), 9(g), 9(h) and 9(i) show the displacement of four measuring point in horizontal and vertical directions, respectively. The motion trajectories of four measuring point in xoy plan are elliptically, as illustrated in Fig. 9(j). However, its ovality and vibrating direction on the rigid frame are different, the reason is that both the magnitudes and phase constants of their displacements are different in horizontal and vertical directions. In addition, some simulation results of corresponding experimental prototype are employed to verify the correctness of theoretical analysis based on Eq.(1). The comparison between the dynamic test results and the simulation results with three co-rotating rotors system are given in Table 4. Those results show that the dynamic test results are proven to be in good agreement with simulation results, and all range of error for the measuring-point in vibrating body are within 30%.

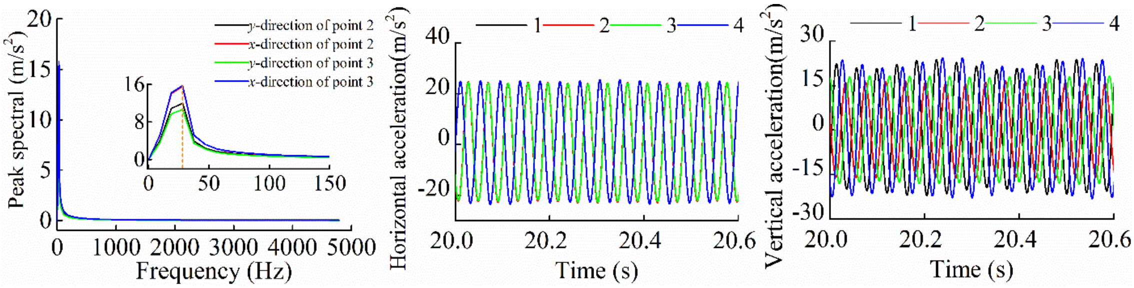

a) b) c)

*Mingjun Du's Address: Southwest Petroleum University, Chengdu, China, dmj9213@163.com

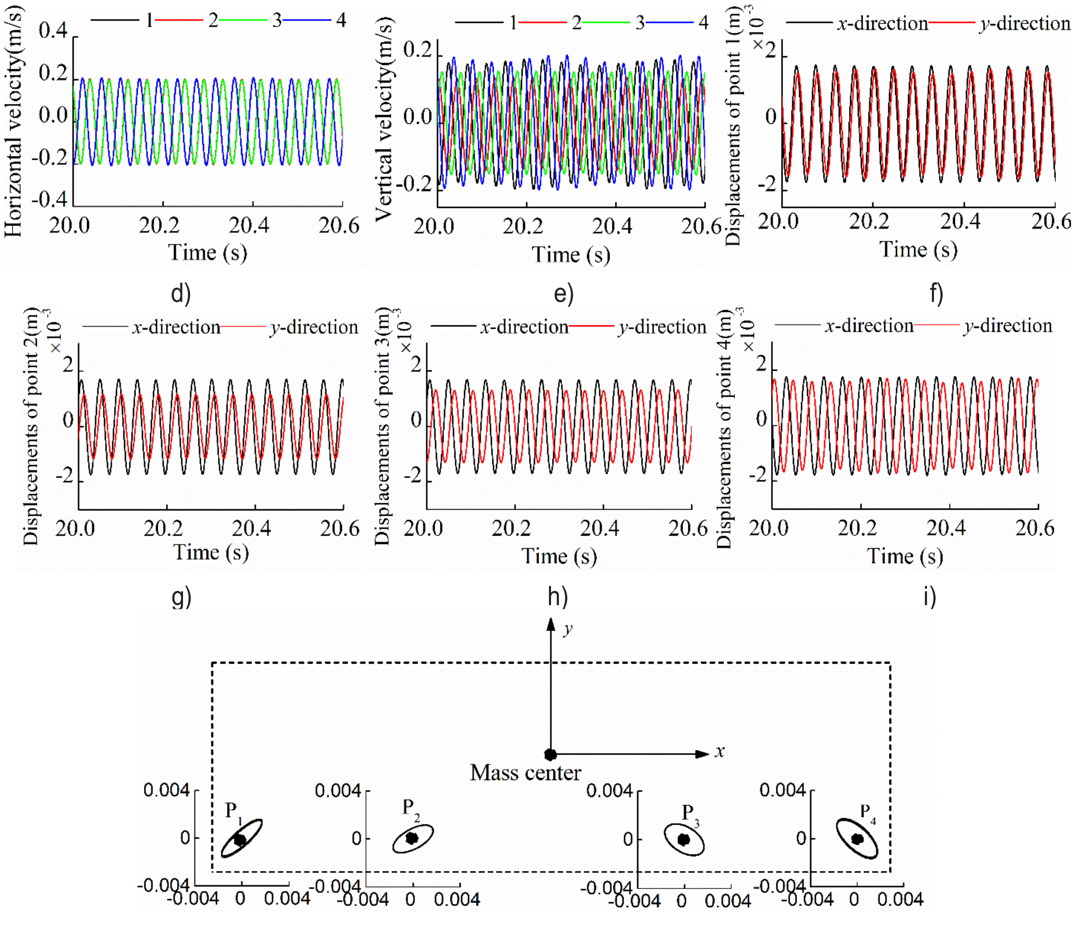

j)

Fig. 9. *Dynamic characteristics of three co-rotating rotors system: a) spectral analysis; b) Horizontal accelerations of the measuring point; c) Vertical accelerations of the measuring point; d) Horizontal velocity of the measuring point; e) Vertical velocity of the measuring point; f) Displacements of the point 1; g) Displacements of the point 2; h) Displacements of the point 3; I) Displacements of the point 4; and j) Motion trail of the measuring point in xoy plane*

Table 4. The amplitude comparison between the dynamic testing results and the simulation results with three co-rotating rotors system

	Results of dynamical testing		Results of dynamical simulation		Error value	
	x- direction	y- direction	x- direction	y- direction	x- direction	y- direction
Measuring point P_1	0.0017	0.0016	0.0015	0.0018	11.8%	11.1%
Measuring point P_2	0.0017	0.0011	0.0014	0.0015	17.6%	26.7%
Measuring point P_3	0.0017	0.0013	0.0014	0.0013	17.6%	0
Measuring point P_4	0.0018	0.0018	0.0015	0.0016	16.7%	11.1%

Strojniški vestnik - Journal of Mechanical Engineering vol(yyyy)no, p-p
Received for review: yyyy-mm-dd

Received revised form: yyyy-mm-dd
DOI code
Original / Review / Short Scientific Paper
Accepted for publication: yyyy-mm-dd

Fig. 10 shows the transiently state of three co-rotating rotors at different moments. As can be seen those diagrams, the value of $\Delta\alpha_{12}$ is 3.56[rad], and the value of $\Delta\alpha_{23}$ is 4.04[rad]. It is concluded that the synchronous state of any two motors is in anti-phase synchronization when the vibrating system operates at the steady-state. Comparing with the simulation results of corresponding experimental prototype, the simulation values of $\Delta\alpha_{12}$ and $\Delta\alpha_{23}$ are 3.46[rad], 3.47[rad], respectively, and their error of magnitudes are within 30%, as shown in Table 5.

Fig. 10. *Phase difference with three co-rotating rotors system*

Table 5. The comparison between the testing value and the simulation value of phase difference with three co-rotating rotors system

	Experimenal test results		The result of computer simulation		Error value	
	$2\alpha_{12}$	$2\alpha_{23}$	$2\alpha_{12}$	$2\alpha_{23}$	$\Delta\alpha_{12}$	$\Delta\alpha_{23}$
Phase difference(rad)	204° ≙ 3.56	-128.8° ≙ 4.04	3.46	3.47	2.8%	14.1%

For the experimental prototype with two co-rotating rotors coupled with springs in a vibrating system, its testing results of dynamic characteristics are shown in Fig. 11. From Fig 11(a) and 11(b), it can be seen that the connecting springs with a stress state occuring periodically can be ensured the synchronous operation of the system, the magnitudes of acceleration of point

*Mingjun Du's Address: Southwest Petroleum University, Chengdu, China, dmj9213@163.com

P_2 and point P_3 in horizontal direction are almost the same with a value 20[m/s^2]. But the magnitudes of their acceleration in vertical direction are greater different with values 44.1[m/s^2] and 19.3[m/s^2], respectively. Integrating once and twice for the acceleration during the running process of the steady-state, respectively, we can obtan the velocity and displacement of point P_2 and point P_3 in horizontal and vertical directions, as shown in Fig 11(c)-(f). Moreover, comparing simulation results of corresponding parameters, it can be seen that the results of dynamic testing and simulation with two co-rotating rotors coupled with springs are in good agreement, as shown in Table 6. Fig. 11(g) shows the motion trajectories of point P_2 and point P_3 during the running process of the system, it is easy found that its motions are elliptically when the vibrating system operates at the steady state. But their ovality and vibrating direction on the rigid frame are different.

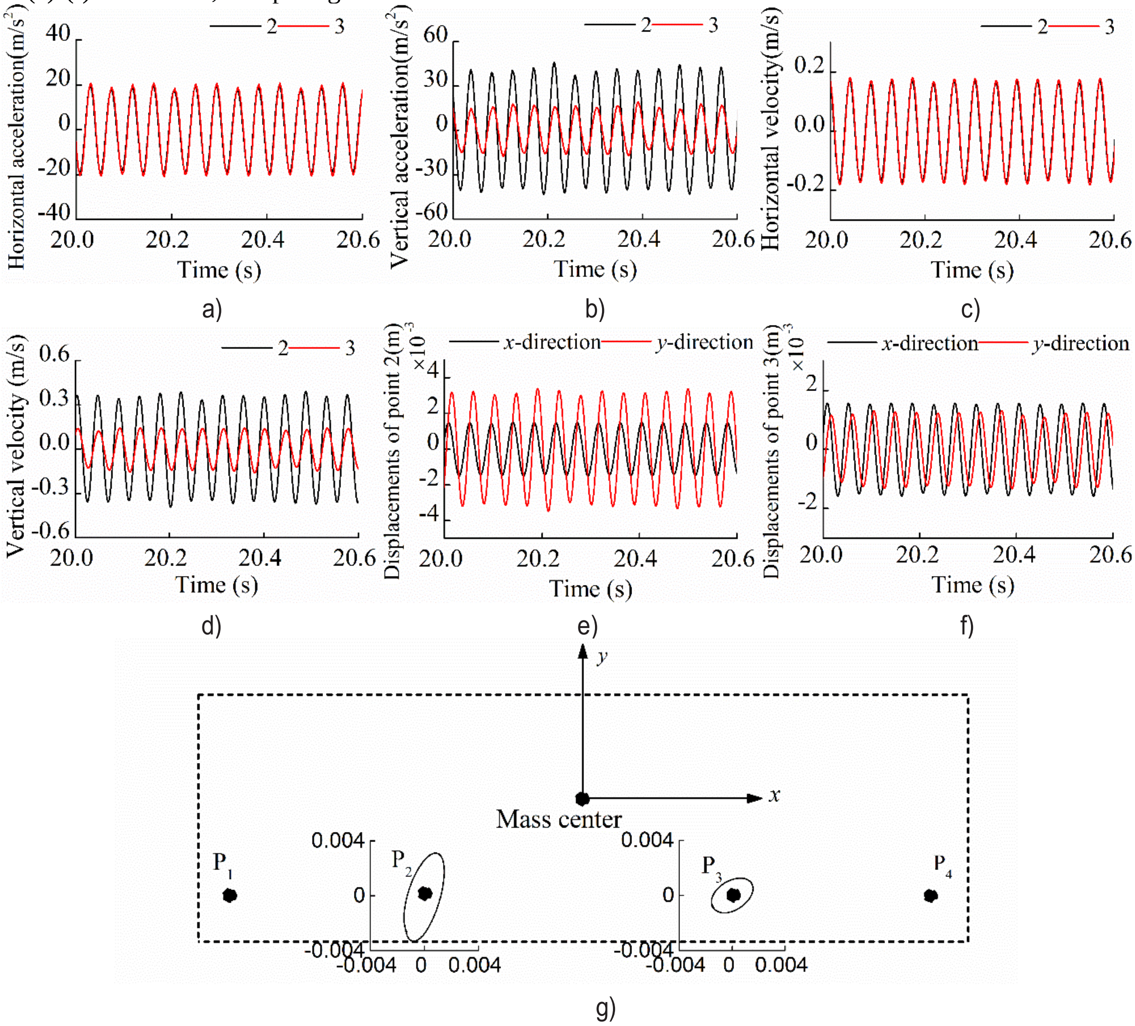

Fig. 11. *Dynamic characteristics of two co-rotating rotors coupled with springs in a vibrating system: a) Horizontal accelerations of the measuring point; b) Vertical accelerations of the measuring point; c) Horizontal velocity of the measuring point; d) Vertical velocity of the measuring point; e) Displacements of the point 2; f) Displacements of the point 3; and g) Motion trail of the measuring point in xoy plane*

Strojniški vestnik - Journal of Mechanical Engineering vol(yyyy)no, p-p
Received for review: yyyy-mm-dd

Received revised form: yyyy-mm-dd
DOI code
Original / Review / Short Scientific Paper
Accepted for publication: yyyy-mm-dd

Table 6. The amplitude comparison between the dynamic testing results and the simulation results with two co-rotating rotors coupled with springs in a vibrating system

	Results of dynamical testing		Results of dynamical simulation		Error value	
	x- direction	y- direction	x- direction	y- direction	x- direction	y- direction
Measuring point P_2	0.0017	0.0016	0.0021	0.0015	19%	23.8%
Measuring point P_3	0.0032	0.0014	0.0027	0.0018	15.6%	22.2%

As can be seen from Fig. 12, the transiently state of two co-rotating rotors coupled with springs are presented by an experimental test. And its comparison between the testing value and the simulation value of phase difference are listed in Table 7. It can be seen that in-phase synchronization of two co-rotating rotors coupled with springs is easy to implement by the springs suffering from the stress state and unstressed state periodically and alternately. That is to say the coupling springs can make the phase difference between the three rotors close to zero during the running process of the steady-state. The experimental results are in good agreement with the simulation results in the vibrating system.

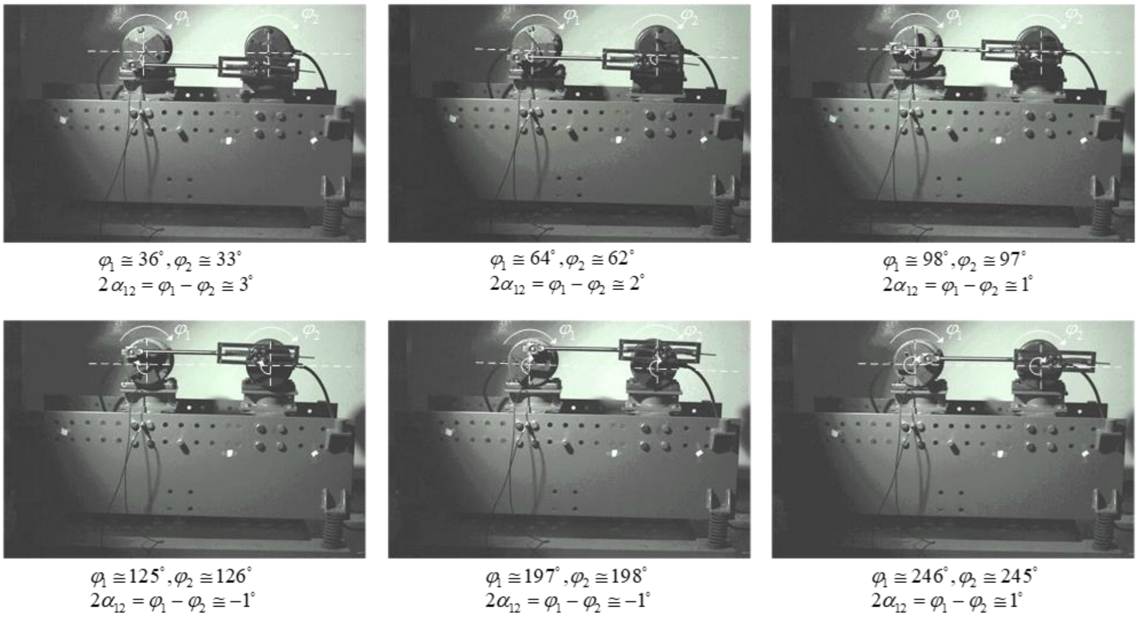

Fig. 12. *Phase difference with two co-rotating rotors coupled with springs in a vibrating system*

Table 7. The comparison between the testing value and the simulation value of phase difference with two co-rotating rotors coupled with springs in a vibrating system

	The results of the indirect experomental tests	The result of computer simulation	Error value
Phase difference $2\alpha_{12}$ (rad)	$0.67° \triangleq 0.012$	$0.75° \triangleq 0.013$	7.7%

5 CONCLUSION

In this work, a vibrating mechanism of three co-rotating rotors system coupled with springs in a non-resonance system is proposed to design large-sized and heavy-duty vibrating screens. The paper is focused on the research of theoretical derivation, numerical analysis,

*Mingjun Du's Address: Southwest Petroleum University, Chengdu, China, dmj9213@163.com

computer simulations and experimental verification. The conclusions are as follows:

(1) For the couping springs with a small stiffness k , the coupling springs have a little influence on synchronization characteristics of the vibrating system. And the synchronous state of motors is always to maintain in anti-phase synchronization. But with the increasing k over a critical value, the phase difference among each two rotors gradually stabilize at zero. Accordingly, synchronous state of the system is changed from anti-phase synchronization to in-phase synchronization. Additionally, it can be concluded that the frequency ratio of the system has a little influence on synchronous behavior, but the synchronous state of the system is influenced by positional parameters of three motors, stiffness coefficient of the coupling springs.

(2) An electromechanical coupled dynamic model of three co-rotating rotors system coupled with springs is established based on the Runge–Kutta algorithm with adaptive control. The relationships between synchronization state of the system and their mechanical-electrical coupling characteristics are investigated. It can be found that the coupling spings with a large enough stiffness can make the phase difference among the three rotors close to zero during the running process of the steady-state. Finally, an experimental prototype including synchronous tests and dynamic tests of the vibrating system is designed to prove to be in good agreement with theory and numerical analysis results.

(3) The presented model in this paper can be applied to large-sized and heavy-duty vibrating screens, which can promote the rapid development of a new drilling technology and the DFSS towards high capacity, high efficiency, low noise, intelligent, energy-saving, environmental protection, etc.

6 ACKNOWLEDGEMENTS

This research was supported by Chengdu International Science and Technology Cooperation Project [No. 2019-GH02-00035-HZ].

7 NOMENCLATURES

m_i	mass of the rotor i , $i=1,2,3$
m_0	mass of the rigid frame
r_i	eccentric radius of the rotor i , $i=1,2,3$
r_0	a standard radius
φ_i	angular displacement of the rotor i , $i=1,2,3$
β_i	installation angle of the rotor i , $i=1,2,3$
l_i	distance from center of mass to the rotor i , $i=1,2,3$
J_i	rotational inertia of the motor i , $i=1,2,3$
f_i	damping coefficient of motor i , $i=1,2,3$
M	the total mass of the vibrating system, $M=m_0+\sum_1^3 m_i$
J	rotational inertia of the vibrating system, $J=J_0+\sum_1^3 m_i l_i^2+\sum_1^3 m_i r_i^2$
f_j	damping constant of the vibrating system in $j-$ direction, $j=x,y,\psi$
k_j	stiffness of four supporting spring in $j-$ direction, $j=x,y,\psi$
k	stiffness coefficient of the connecting spring
a	distance between the rotating center of motor i and the end of coupling springs
α_{12}	phase differences between motor 1 and motor 2
α_{23}	phase differences between motor 2 and motor 3
ε_i	instantaneous change coefficients, $i=1,2,3$
ς_0 , ς_{12} , ς_{23}	coefficients of the instantaneous change with ω_m , α_{12} and α_{23}
$\varsigma_x,\varsigma_y,\varsigma_\psi$	damping coefficient of the vibrating system in $j-$ direction, $j=x,y,\psi$, $\varsigma_x=f_x/2\omega_{nx}M$, $\varsigma_y=f_y/2\omega_{ny}M$, $\varsigma_\psi=f_\psi/2\omega_{n\psi}J$
ω_{nj}	natural frequency of the vibrating system in $j-$direction, $j=x,y,\psi$, $\omega_{nx}=\sqrt{k_x/M}$,

Received for review: yyyy-mm-dd
Received revised form: yyyy-mm-dd
Accepted for publication: yyyy-mm-dd

	$\omega_{ny} = \sqrt{k_y/M}$, $\omega_{n\psi} = \sqrt{k_\psi/J}$
r_m l_e r_{li} r_{ri} η_i	dimensionless parameters $r_m = m_0/M$, $l_e = \sqrt{J/M}$, $r_{li} = l_i/l_e$, $r_{ri} = r_i/r_0$, $\eta_i = m_i/m_0$, $i = 1,2,3$
n_j	frequency ratio in $j-$ direction $n_j = \omega_m/\omega_{nj}$
T_{ei}	driving torque of the rotor i , $i = 1,2,3$
T_{e0i}	output torque of the rotor i , $i = 1,2,3$
$\bar{k}_{e0i}$	scaling factor of electrical and mechanical damping, $i = 1,2,3$
T	total kinetic energy of the system
V	total potential energy of the system
Q_i	generalized force of the system
q_i	generalized coordinate of the system
T_z	the sum of kinetic energy with three motors
$\langle \bar{\bullet} \rangle$	integrating over one period T of time, $\langle \bar{\bullet} \rangle = \int_T^{t_0+T} (\bullet) dt$
$(\dot{\bullet})$	The first derivative of time, $d(\bullet)/dt$
$(\ddot{\bullet})$	The second derivative of time, $d^2(\bullet)/dt^2$

8 REFERENCES

[1] Baragetti, S. (2015). Innovative structural solution for heavy loaded vibrating screens. *Minerals Engineering,* vol. 84, p. 15-26, DOI: 10.1016/j.mineng.2015.09.011.

[2] Dong, K., Esfandiary, A.H., Yu, A.B. (2017). Discrete particle simulation of particle flow and separation on a vibrating screen: Effect of aperture shape. *Powder Technology,* vol. 314, p. 195-202, DOI: 10.1016/j.powtec.2016.11.004.

[3] Dong, K.J., Yu, A.B. (2012). Numerical simulation of the particle flow and sieving behaviour on sieve bend/low head screen combination. *Minerals Engineering,* vol. 31, no. 4, p. 2-9, DOI: 10.1016/j.mineng.2011.10.020.

[4] Blekhman, I.I. (1988). *Synchronization in science and technology*. ASME Press,

[5] Blekhman, I.I., Sorokin, V.S. (2018). On a "deterministic" explanation of the stochastic resonance phenomenon. *Nonlinear Dynamics,* vol. 93, no. 2, p. 767-778, DOI: 10.1007/s11071-018-4225-y.

[6] Blekhman, I.I., Sorokin, V.S. (2010). On the separation of fast and slow motions in mechanical systems with high-frequency modulation of the dissipation coefficient. *Journal of Sound and Vibration,* vol. 329, no. 23, p. 4936-4949, DOI: 10.1016/j.jsv.2010.06.008.

[7] Balthazar, J.M., Felix, J.L.P., Brasil, R.M. (2005). Some comments on the numerical simulation of self-synchronization of four non-ideal exciters. *Applied Mathematics & Computation,* vol. 164, no. 2, p. 615–625.

[8] Balthazar, J.M., Felix, J.L.P., Brasil, R.M.L.R.F. (2016). Short comments on self-synchronization of two non-ideal sources supported by a flexible portal frame structure. *Journal of Vibration and Control,* vol. 10, no. 12, p. 1739-1748, DOI: 10.1177/1077546304041754.

[9] Wen, B., Fan, J., Zhao, C., Xiong, W. (2012). Vibratory and controlled synchronization engineering.

[10] Wen, B., Zhang, H., Liu, S., He, Q., Zhao, C. (2010). *Theory and techniques of vibrating machinery and their applications*. Science Press, Beijing.

[11] Zhang, X.L., Wen, B.C., Zhao, C.Y. (2013). Synchronization of three non-identical coupled exciters with the same rotating directions in a far-resonant vibrating system. *Journal of Sound and Vibration,* vol. 332, no. 9, p. 2300-2317, DOI: 10.1016/j.jsv.2012.12.003.

[12] Zhang, X., Wen, B., Zhao, C. (2014). Vibratory synchronization transmission of two exciters in a super-resonant vibrating system. *Journal of Mechanical Science and Technology,* vol. 28, no. 6, p. 2049-2058, DOI: 10.1007/s12206-014-0108-4.

[13] Fang, P., Hou, Y.J. (2018). Synchronization characteristics of a rotor-pendula system in multiple coupling resonant systems. *Proceedings of the Institution of Mechanical Engineers Part C-Journal of Mechanical*

*Mingjun Du's Address: Southwest Petroleum University, Chengdu, China, dmj9213@163.com

Engineering Science, vol. 232, no. 10, p. 1802-1822, DOI: 10.1177/0954406217711468.

[14] Fang, P., Hou, Y.J., Du, M.J. (2019). Synchronization behavior of triple-rotor-pendula system in a dual-super-far resonance system. *Proceedings of the Institution of Mechanical Engineers Part C-Journal of Mechanical Engineering Science,* vol. 233, no. 5, p. 1620-1640, DOI: 10.1177/0954406218774585.

[15] Chen, X., Kong, X., Liu, Y., Wen, B. (2016). Synchronization and coupling dynamic characteristics of a dual-rotors exciter. *Journal of Vibroengineering,* vol. 18, no. 5, p. 3318-3328.

[16] Chen, X.Z., Kong, X.X., Zhang, X.L., Li, L.X., Wen, B.C. (2016). On the synchronization of two eccentric rotors with common rotational axis: Theory and experiment. *Shock and Vibration,* vol. 2016, DOI: Artn 697359710.1155/2016/6973597.

[17] Huang, Z.L., Song, G.Q., Li, Y.M., Sun, M.N. (2019). Synchronous control of two counter-rotating eccentric rotors in nonlinear coupling vibration system. *Mechanical Systems and Signal Processing,* vol. 114, p. 68-83, DOI: 10.1016/j.ymssp.2018.05.006.

[18] Huang, Z., Song, G., Zhang, Z., Zhang, X. (2019). Control synchronization of two nonidentical homodromy exciters in nonlinear coupled vibration system. *IEEE Access,* vol. 7, p. 109934-109944, DOI: 10.1109/access.2019.2933033.

[19] Kong, X.X., Chen, C.Z., Wen, B.C. (2018). Composite synchronization of three eccentric rotors driven by induction motors in a vibrating system. *Mechanical Systems and Signal Processing,* vol. 102, p. 158-179, DOI: 10.1016/j.ymssp.2017.09.025.

[20] Kong, X.X., Zhang, X.L., Chen, X.Z., Wen, B.C., Wang, B. (2016). Phase and speed synchronization control of four eccentric rotors driven by induction motors in a linear vibratory feeder with unknown time-varying load torques using adaptive sliding mode control algorithm. *Journal of Sound and Vibration,* vol. 370, p. 23-42, DOI: 10.1016/j.jsv.2016.02.013.

[21] Huang, Z.L., Li, Y.M., Song, G.Q., Zhang, X.L., Zhang, Z.C. (2019). Speed and phase adjacent cross-coupling synchronous control of multi-exciters in vibration system considering material influence. *Ieee Access,* vol. 7, p. 63204-63216, DOI: 10.1109/Access.2019.2916983.

[22] Zhang, X., Wen, B., Zhao, C. (2014). Vibratory synchronization and coupling dynamic characteristics of multiple unbalanced rotors on a mass-spring rigid base. *International Journal of Non-Linear Mechanics,* vol. 60, p. 1-8, DOI: 10.1016/j.ijnonlinmec.2013.12.002.

[23] Hou, Y. (2007). The synchronism theory of three motor self-synchronism exciting elliptical motion shaker. *Joumal of Southwest Petroleum University,* vol. 29, p. 168-172.

9 APPENDIX

$$\rho_{11}=\frac{J_1}{m_0 r_0^{\,2}}+\frac{1}{2}\eta_1^{\,2} r_{r1}^{\,2} W_{c1}$$

$$\rho_{12}=\frac{J_2}{m_0 r_0^{\,2}}+\frac{1}{2}\eta_2 r_{r2}\eta_2 r_{r2} W_{c2}$$

$$\rho_{13}=\frac{J_3}{m_0 r_0^{\,2}}+\frac{1}{2}\eta_3 r_{r3}\eta_3 r_{r3} W_{c3}$$

$$\chi_{12}'=\frac{1}{2}\eta_1\eta_2 r_{r1} r_{r2}\begin{bmatrix} W_{c12}\cos\left(\alpha_{12}+\theta_{c12}\right) \\ -W_{s12}\sin\left(\alpha_{12}+\theta_{s12}\right)\end{bmatrix}$$

$$\chi_{13}'=\frac{1}{2}\eta_1\eta_3 r_{r1} r_{r3}\begin{bmatrix} W_{c13}\cos\left(\alpha_{12}+\alpha_{23}+\theta_{c13}\right)- \\ W_{s13}\sin\left(\alpha_{12}+\alpha_{23}+\theta_{s13}\right)\end{bmatrix}$$

$$k_{11}=\frac{\bar{k}_{e01}}{m_0 r_0^{\,2}\omega_m^{\,2}}+\frac{f_1}{m_0 r_0^{\,2}\omega_m}+\eta_1^{\,2} r_{r1}^{\,2} W_{s1}$$

$$k_{22}=\frac{\bar{k}_{e02}}{m_0 r_0^{\,2}\omega_m^{\,2}}+\frac{f_2}{m_0 r_0^{\,2}\omega_m}+\eta_2^{\,2} r_{r2}^{\,2} W_{s2}$$

$$k_{33}=\frac{\bar{k}_{e03}}{m_0 r_0^{\,2}\omega_m^{\,2}}+\frac{f_3}{m_0 r_0^{\,2}\omega_m}+\eta_3 r_{r3}\eta_3 r_{r3} W_{s3}$$

Strojniški vestnik - Journal of Mechanical Engineering vol(yyyy)no, p-p
Received for review: yyyy-mm-dd

Received revised form: yyyy-mm-dd
DOI code
Original / Review / Short Scientific Paper
Accepted for publication: yyyy-mm-dd

$$\chi_{12} = \eta_1 r_{r1} \eta_2 r_{r2} \begin{bmatrix} W_{c12} \sin\left(\alpha_{12} + \theta_{c12}\right) \\ +W_{s12} \cos\left(\alpha_{12} + \theta_{s12}\right) \end{bmatrix}$$

$$\chi_{13} = \eta_1 r_{r1} \eta_3 r_{r3} \begin{bmatrix} W_{c13} \sin\left(\alpha_{12} + \alpha_{23} + \theta_{c13}\right) \\ +W_{s13} \sin\left(\alpha_{12} + \alpha_{23} + \theta_{s13}\right) \end{bmatrix}$$

$$\begin{aligned} \mu_1 = {} & \frac{T_{e01}}{m_0 {r_0}^2 \omega_m} - \frac{f_1}{m_0 {r_0}^2} - \frac{1}{2} \eta_1 r_{r1} \eta_1 r_{r1} \omega_m W_{s1} \\ & - \frac{1}{2} \eta_1 r_{r1} \eta_2 r_{r2} \omega_m \begin{bmatrix} W_{c12} \sin\left(\alpha_{12} + \theta_{c12}\right) \\ +W_{s12} \cos\left(\alpha_{12} + \theta_{s12}\right) \end{bmatrix} \\ & - \frac{1}{2} \eta_1 r_{r1} \eta_3 r_{r3} \omega_m \begin{bmatrix} W_{c13} \sin\left(\alpha_{12} + \alpha_{23} + \theta_{c13}\right) \\ +W_{s13} \sin\left(\alpha_{12} + \alpha_{23} + \theta_{s13}\right) \end{bmatrix} \\ & - \frac{ka^2}{m_0 {r_0}^2 \omega_m} \sin \alpha_{12} + \frac{F_1}{m_0 {r_0}^2} \end{aligned}$$

$$\chi'_{21} = \frac{1}{2} \eta_2 r_{r2} \eta_1 r_{r1} \begin{bmatrix} W_{c12} \cos\left(\alpha_{12} + \theta_{c12}\right) \\ +W_{s12} \sin\left(\alpha_{12} + \theta_{s12}\right) \end{bmatrix}$$

$$\chi'_{23} = \frac{1}{2} \eta_2 r_{r2} \eta_3 r_{r3} \begin{bmatrix} W_{c23} \cos\left(\alpha_{23} + \theta_{c23}\right) \\ -W_{s23} \sin\left(\alpha_{23} + \theta_{s23}\right) \end{bmatrix}$$

$$\chi_{21} = -\eta_2 r_{r2} \eta_1 r_{r1} \begin{bmatrix} W_{c12} \sin\left(\alpha_{12} + \theta_{c12}\right) \\ -W_{s12} \cos\left(\alpha_{12} + \theta_{s12}\right) \end{bmatrix}$$

$$\chi_{23} = \eta_2 \eta_3 r_{r2} r_{r3} \begin{bmatrix} W_{c23} \sin\left(\alpha_{23} + \theta_{c23}\right) \\ +W_{s23} \cos\left(\alpha_{23} + \theta_{s23}\right) \end{bmatrix}$$

$$\begin{aligned} \mu_2 = {} & \frac{T_{e02}}{m_0 {r_0}^2 \omega_m} - \frac{f_2}{m_0 {r_0}^2} \\ & + \frac{1}{2} \eta_1 \eta_2 r_{r1} r_{r2} \omega_m \begin{bmatrix} W_{c12} \sin\left(\alpha_{12} + \theta_{c12}\right) \\ -W_{s12} \cos\left(\alpha_{12} + \theta_{s12}\right) \end{bmatrix} \\ & - \frac{1}{2} {\eta_2}^2 {r_{r2}}^2 \omega_m W_{s2} \\ & - \frac{1}{2} \eta_2 \eta_3 r_{r2} r_{r3} \omega_m \begin{bmatrix} W_{c23} \sin\left(\alpha_{23} + \theta_{c23}\right) \\ +W_{s23} \cos\left(\alpha_{23} + \theta_{s23}\right) \end{bmatrix} \\ & + \frac{ka^2}{m_0 {r_0}^2 \omega_m} \left(\sin \alpha_{12} - \sin \alpha_{23}\right) + \frac{F_2}{m_0 {r_0}^2} \end{aligned}$$

$$\chi'_{31} = \frac{1}{2} \eta_3 r_{r3} \eta_1 r_{r1} \begin{bmatrix} W_{c13} \cos\left(\alpha_{12} + \alpha_{23} + \theta_{c13}\right) \\ +W_{s13} \sin\left(\alpha_{12} + \alpha_{23} + \theta_{s13}\right) \end{bmatrix}$$

$$\chi'_{32} = \frac{1}{2} \eta_3 r_{r3} \eta_2 r_{r2} \begin{bmatrix} W_{c23} \cos\left(\alpha_{23} + \theta_{c23}\right) \\ +W_{s23} \sin\left(\alpha_{23} + \theta_{s23}\right) \end{bmatrix}$$

$$\chi_{31} = -\eta_3 r_{r3} \eta_1 r_{r1} \begin{bmatrix} W_{c13} \sin\left(\alpha_{12} + \alpha_{23} + \theta_{c13}\right) \\ -W_{s13} \cos\left(\alpha_{12} + \alpha_{23} + \theta_{s13}\right) \end{bmatrix}$$

$$\chi_{32} = -\eta_3 r_{r3} \eta_2 r_{r2} \begin{bmatrix} W_{c23} \sin\left(\alpha_{23} + \theta_{c23}\right) \\ -W_{s23} \cos\left(\alpha_{23} + \theta_{s23}\right) \end{bmatrix}$$

$$\begin{aligned} \mu_3 = {} & \frac{T_{e03}}{m_0 {r_0}^2 \omega_m} - \frac{f_3}{m_0 {r_0}^2} \\ & + \frac{1}{2} \eta_3 r_{r3} \eta_1 r_{r1} \omega_m \begin{bmatrix} W_{c13} \sin\left(\alpha_{12} + \alpha_{23} + \theta_{c13}\right) \\ -W_{s13} \cos\left(\alpha_{12} + \alpha_{23} + \theta_{s13}\right) \end{bmatrix} \\ & + \frac{1}{2} \eta_3 r_{r3} \eta_2 r_{r2} \omega_m \begin{bmatrix} W_{c23} \sin\left(\alpha_{23} + \theta_{c23}\right) \\ -W_{s23} \cos\left(\alpha_{23} + \theta_{s23}\right) \end{bmatrix} \\ & - \frac{1}{2} \eta_3 r_{r3} \eta_3 r_{r3} \omega_m W_{s3} + \frac{ka^2}{m_0 {r_0}^2 \omega_m} \sin \alpha_{23} + \frac{F_3}{m_0 {r_0}^2} \end{aligned}$$

$$W_{c1} = r_m \left[\mu_x \cos \gamma_x + \mu_y \cos \gamma_y + \mu_\psi {r_{l1}}^2 \cos \gamma_\psi \right]$$

$$W_{c2} = r_m \left[\mu_x \cos \gamma_x + \mu_y \cos \gamma_y + \mu_\psi {r_{l2}}^2 \cos \gamma_\psi \right]$$

$$W_{c3} = r_m \left[\mu_x \cos \gamma_x + \mu_y \cos \gamma_y + \mu_\psi {r_{l3}}^2 \cos \gamma_\psi \right]$$

$$W_{s1} = r_m \left[\mu_x \sin \gamma_x + \mu_y \sin \gamma_y + \mu_\psi {r_{l1}}^2 \sin \gamma_\psi \right]$$

$$W_{s2} = r_m \left[\mu_x \sin \gamma_x + \mu_y \sin \gamma_y + \mu_\psi {r_{l2}}^2 \sin \gamma_\psi \right]$$

$$W_{s3} = r_m \left[\mu_x \sin \gamma_x + \mu_y \sin \gamma_y + \mu_\psi {r_{l3}}^2 \sin \gamma_\psi \right]$$

$$\begin{aligned} a_{s12} = {} & \mu_x \sin \gamma_x + \mu_y \sin \gamma_y \\ & + \mu_\psi r_{l1} r_{l2} \sin \gamma_\psi \cos\left(\beta_1 - \beta_2\right) \end{aligned}$$

$$b_{s12} = \mu_\psi r_{l1} r_{l2} \sin \gamma_\psi \sin\left(\beta_1 - \beta_2\right)$$

$$W_{s12} = r_m \sqrt{{a_{s12}}^2 + {b_{s12}}^2}$$

$$\theta_{s12} = \begin{cases} \arctan(b_{s12} / a_{s12}) & a_{s12} \geq 0 \\ \pi + \arctan(b_{s12} / a_{s12}) & a_{s12} < 0 \end{cases}$$

$$\begin{aligned} a_{s13} = {} & \mu_x \sigma \sin \gamma_x + \mu_y \sin \gamma_y \\ & + \mu_\psi r_{l1} r_{l3} \sin \gamma_\psi \cos(\beta_1 - \sigma \beta_3) \end{aligned}$$

$$b_{s13} = \mu_\psi r_{l1} r_{l3} \sin \gamma_\psi \sin(\beta_1 - \sigma \beta_3)$$

$$W_{s13} = r_m \sqrt{{a_{s13}}^2 + {b_{s13}}^2}$$

$$\theta_{s13} = \begin{cases} \arctan(b_{s13} / a_{s13}) & a_{s13} \geq 0 \\ \pi + \arctan(b_{s13} / a_{s13}) & a_{s13} < 0 \end{cases}$$

*Mingjun Du's Address: Southwest Petroleum University, Chengdu, China, dmj9213@163.com

$$a_{s23} = \mu_x \sigma \sin\gamma_x + \mu_y \sin\gamma_y + \mu_\psi r_{l2} r_{l3} \sin\gamma_\psi \cos(\beta_2 - \sigma\beta_3)$$

$$b_{s23} = \mu_\psi r_{l2} r_{l3} \sin\gamma_\psi \sin(\beta_2 - \sigma\beta_3)$$

$$W_{s23} = r_m \sqrt{a_{s23}^2 + b_{s23}^2}$$

$$\theta_{s23} = \begin{cases} \arctan(b_{s23}/a_{s23}) & a_{s23} \geq 0 \\ \pi + \arctan(b_{s23}/a_{s23}) & a_{s23} < 0 \end{cases}$$

$$a_{c12} = \mu_x \cos\gamma_x + \mu_y \cos\gamma_y + \mu_\psi r_{l1} r_{l2} \cos\gamma_\psi \cos(\beta_1 - \beta_2)$$

$$b_{c12} = \mu_\psi r_{l1} r_{l2} \cos\gamma_\psi \sin(\beta_1 - \beta_2)$$

$$W_{c12} = r_m \sqrt{a_{c12}^2 + b_{c12}^2}$$

$$\theta_{c12} = \begin{cases} \arctan(b_{c12}/a_{c12}) & a_{c12} \geq 0 \\ \pi + \arctan(b_{c12}/a_{c12}) & a_{c12} < 0 \end{cases}$$

$$a_{c13} = \mu_x \sigma \cos\gamma_x + \mu_y \cos\gamma_y + \mu_\psi r_{l1} r_{l3} \cos\gamma_\psi \cos(\beta_1 - \sigma\beta_3)$$

$$b_{c13} = \mu_\psi r_{l1} r_{l3} \cos\gamma_\psi \sin(\beta_1 - \sigma\beta_3)$$

$$W_{c13} = r_m \sqrt{a_{c13}^2 + b_{c13}^2}$$

$$\theta_{c13} = \begin{cases} \arctan(b_{c13}/a_{c13}) & a_{c13} \geq 0 \\ \pi + \arctan(b_{c13}/a_{c13}) & a_{c13} < 0 \end{cases};$$

$$a_{c23} = \mu_x \sigma \cos\gamma_x + \mu_y \cos\gamma_y + \mu_\psi r_{l2} r_{l3} \cos\gamma_\psi \cos(\beta_2 - \sigma\beta_3)$$

$$b_{c23} = \mu_\psi r_{l2} r_{l3} \cos\gamma_\psi \sin(\beta_2 - \sigma\beta_3)$$

$$W_{c23} = r_m \sqrt{a_{c23}^2 + b_{c23}^2}$$

$$\theta_{c23} = \begin{cases} \arctan(b_{c23}/a_{c23}) & a_{c23} \geq 0 \\ \pi + \arctan(b_{c23}/a_{c23}) & a_{c23} < 0 \end{cases}$$

$$f_1(k,\varphi_1,\varphi_2,\varphi_3,\beta,l,a) = \frac{-a^2 \sin(\varphi_2 - \varphi_1) + la\cos\varphi_1 \cos\beta}{\sqrt{l^2\cos^2\beta + 2a^2 - 2a^2\cos(\varphi_2 - \varphi_1) + 2la\sin\varphi_1\cos\beta - 2la\sin\varphi_2\cos\beta}}$$

$$f_2(k,\varphi_1,\varphi_2,\varphi_3,\beta,l,a) = \frac{a^2 \sin(\varphi_2 - \varphi_1) - la\cos\varphi_2 \cos\beta}{\sqrt{l^2\cos^2\beta + 2a^2 - 2a^2\cos(\varphi_2 - \varphi_1) + 2la\sin\varphi_1\cos\beta - 2la\sin\varphi_2\cos\beta}} + \frac{-a^2 \sin(\varphi_3 - \varphi_2) + la\cos\varphi_2 \cos\beta}{\sqrt{l^2\cos^2\beta + 2a^2 - 2a^2\cos(\varphi_3 - \varphi_2) + 2la\sin\varphi_2\cos\beta - 2la\sin\varphi_3\cos\beta}}$$

$$f_3(k,\varphi_1,\varphi_2,\varphi_3,\beta,l,a) = \frac{a^2 \sin(\varphi_3 - \varphi_2) - la\cos\varphi_3 \cos\beta}{\sqrt{l^2\cos^2\beta + 2a^2 - 2a^2\cos(\varphi_3 - \varphi_2) + 2la\sin\varphi_2\cos\beta - 2la\sin\varphi_3\cos\beta}}$$

$$F_1 = \frac{1}{2\pi}\int_0^{2\pi} f_1(k,\varphi_1,\varphi_2,\varphi_3,\beta,l,a)\,d\varphi$$

$$F_2 = \frac{1}{2\pi}\int_0^{2\pi} f_2(k,\varphi_1,\varphi_2,\varphi_3,\beta,l,a)\,d\varphi$$

$$F_3 = \frac{1}{2\pi}\int_0^{2\pi} f_3(k,\varphi_1,\varphi_2,\varphi_3,\beta,l,a)\,d\varphi$$